THE INDIAN MINING & ENGINEERING JOURNAL

(Incorporating Mineral Markets: The Founder Publisher & Editor: J.F. De. Souza, Mumbai)

VOLUME 64: No.08-09 **AUGUST-SEPTEMBER 2025** ISSN 0019-5944

(PEER REVIEWED JOURNAL DEVOTED TO MINING, EARTH SCIENCES & ENGINEERING)

Contents
Technical Papers

03. Numerical Simulation of the Effect of Fault on Pit Slope Stability
V K Singh, Nancy Dung Dung, Rajesh Rai & Ashok Jaiswal

10. Genomic, Hydrogeomorphic, And Linguistic Syntaxis in the Indus Valley Civilization: Insights from Rakhigarhi Adna to Keezhadi and Quaternary Proxies
Dr. Ashokaditya P. Dhurandhar

33. Controlled Blasting Parameter Optimization to Ensure Safety and Efficiency in Opencast Mine Operations
Amar Prakash Kaushik, Vivek Kumar Himanshu, Ashutosh Kumar Dwivedi & Ashish Mishra

www.theimejournal.com
Publisher : Anita Pradhan, IME Publications

Editor-in-Chief: Prof. **S.Jayanthu**,
National Mineral Awardee, Deptt. of Mining, NIT, Rourkela
Mob. 9938303259 , Email: sjayanthu@nitrkl.ac.in

Editor: S.K.Mahanta,
Mob.: 9437002349
Email: sushantamahanta2349@gmail.com

IME PUBLICATIONS

Corresspondance Address
The IM& E Journal 1457, Fishery Tank Road, Chintamaniswar, Laxmisagarpatna, Bhubaneswar - 751006, Odisha
Mobile: +919861008387, **Mail:** indianminingjournal61@hotmail.com / indianminingjournal@gmail.com
Branch office:Near TV Tower, JODA, Dt. Keonjhar 758034, Phone: 06767-273173
Associate Editor: A.Sahoo, Mob. 9861008387

EDITORIAL TEAM MEMBERS & REVIEWERS

Acknowledgement:

The papers published in this volume were also presented at the International Conference on Safe & Sustainable Mining Technologies, IConSSMT 2024 held at AKS University, Satna (M.P) during19-21 February 2024. The two technical papers, Climate Change - Sustainable Mining and Need for Accelerated Development of Coal by D N Prasad and Rock Fragemntation Research in Mining & Port Construction- Some Applications, by Prof. V.M.S.R. Murthy were the Key Note Papers. Authors who have not attended the Conference, their papers were not published in this volume.

The Indian Mining & Engineering Journal, Vol. 64, No.08-09 August-September 2025, pp.03-09
Printed in India, @ IME Publications, ISSN 0019-5944

Numerical Simulation of the Effect of Fault on Pit Slope Stability

V K Singh* Nancy Dung Dung** Rajesh Rai** Ashok Jaiswal**

ABSTRACT

Faults can have a substantial impact on pit slope stability in open-pit mining operations because they can create zones of weakness that can lead to slope failure. The effect of faults on slope stability depends on several factors, including fault type, orientation, and the geological and geotechnical conditions of the adjoining rock mass.

In the present paper, the effect of fault on rock slope has been analyzed. The location and the angle of the fault have been analyzed using numerical modelling. The critical distance between the crest and the fault has been determined. The Geotechnical properties of fault and rock mass have been varied to find out the effect of geotechnical properties on rock slope.

INTRODUCTION

The effect of faults on pit slope stability in open-pit mining operations can be significant, as faults can create zones of weakness that can lead to slope failure. The impact of faults on slope stability can vary depending on a variety of factors, including the type of fault, its orientation, and the geological and geotechnical conditions of the surrounding rock. The fault direction appears as a critical predictor of slope stability outcomes (Ntšolo, 2017). A fault parallel to the slope might cause gradual failures, whereas one perpendicular to the slope can cause sudden collapses or slides. This unpredictability adds a degree of complication to slope stability studies.

The impact of faults is not a one-size-fits-all scenario; rather, it is contingent upon a multitude of factors, including fault type, orientation, and proximity to the pit slope. This complexity arises from the way faults create zones of weakness within the rock mass, thereby altering the stability dynamics (Erso, 2021).

Normal faults generate steeply dipping planes of weakness that can connect with the slope and reduce its overall stability. However, reverse faults can create zones of compression that increase the strength of the rock mass and make the slope more stable (Kolapo,2022). Strike-slip faults can complicate matters by generating shearing and movement zones that can have unanticipated consequences. Strike-slip faults can increase the complex by causing shearing and movement zones that could have unanticipated consequences for the stability of the slope (Zhang, 2021, Azarfar,2018)

Faults can also affect the pressure and movement of groundwater within the rock mass, which can further reduce the stability of the slope. The pore pressure and shear strength of the surrounding rock can alter as a result of faults creating pathways for groundwater to pass through (Zhang, 2021). This may increase the slope's vulnerability to failure, particularly in the event of an abrupt shift in water pressure, intense precipitation, or seismic activity.

Pit slope stability is often evaluated by employing geological mapping, numerical modelling, and geotechnical monitoring. Determining the location, orientation, and features of faults within a rock mass can be facilitated by geological mapping. Geotechnical monitoring can be used to track changes in slope behaviour over time, such as variations in groundwater pressure or surface deformation (Kuraoka, 2000). It ensures the safety of slope mass. Long-term sustainability of open-pit mining operations requires an understanding of how faults affect the pit slope stability.

Pit slope stability in mining operations is very important because the stability of excavated slopes is critical to the safety and efficiency of these activities. The stable pit slope is critical for preventing accidents, ensuring worker safety, and avoiding production disruptions (Zeng, 2013). Geological considerations play an important role in shaping the stability of these slopes, with faults developing

** Retd. Chief Scientist, CIMFR, Dhanbad*
***Department of Mining Engineering, Indian Institute of Technology, (Banaras Hindu University), Varanasi, 221005*

as a prominent geological feature that can have an enormous effect on slope stability (Kristiono, 2015)

Geological faults play a role in slope stability because these are fractures in the Earth's crust along which rocks have moved relative to one another. The scale, position, and displacement of these faults might vary. When discussing pit slope stability, faults bring complexity that can have a substantial impact on the slopes' overall stability. Faults can operate as potential failure planes or zones of weakness, modifying stress distribution within the rock mass and influencing slope mechanical behaviour (Zhang, 2021). The existence of faults can result in increased pore pressure, decreased cohesiveness, and altered frictional properties, all of which contribute to changes in slope stability.

In the present paper, "Effect of Faults on Slope Stability" has been taken for a research study. RS2 software based on the finite element method has been used to investigate the effect of fault. Various parameters have been varied.

SIMULATION AND VALIDATION OF THE NUMERICAL MODEL

The fault generally initiates plane failure in the rock slope. The factor of safety of plane failure can be determined by the limit equilibrium method. A well-developed formulation is given in many books (Wyllie, 2004). In the present study, the finite element method has been used to simulate the influence of fault on slope stability. The first step is to validate the models using FEM. The three models have been made using RS2 software based on the finite element method and the same model is also solved by RocPlane software (based on the limit equilibrium method).

Figure 1 shows the discretized model of slope ass with 80^0 slope angle and fault plane of 50^0. Figure 2 shows the fault slope model with the Rocplan software. Table 1 shows details of all three models. All three models have a slope angle of 80 degrees, a bench height of 20 meters, and fault angles of 40, 45, and 50 degrees, respectively. The cohesion values for these models are 20 KPa, 100 KPa, and 50 KPa, while the friction angles are set at 40, 45, and 50 degrees, respectively. The factor of safety calculations have been performed using Rocscience Plane and Rocscience Phase 2 software.

Table 1 shows the factor of safety results from both programs, RS2 (FEM) and Rock Plane (LEM). The factor of safety values obtained from both software are very close to each other. This similarity indicates that the model is accurate and has been successfully validated.

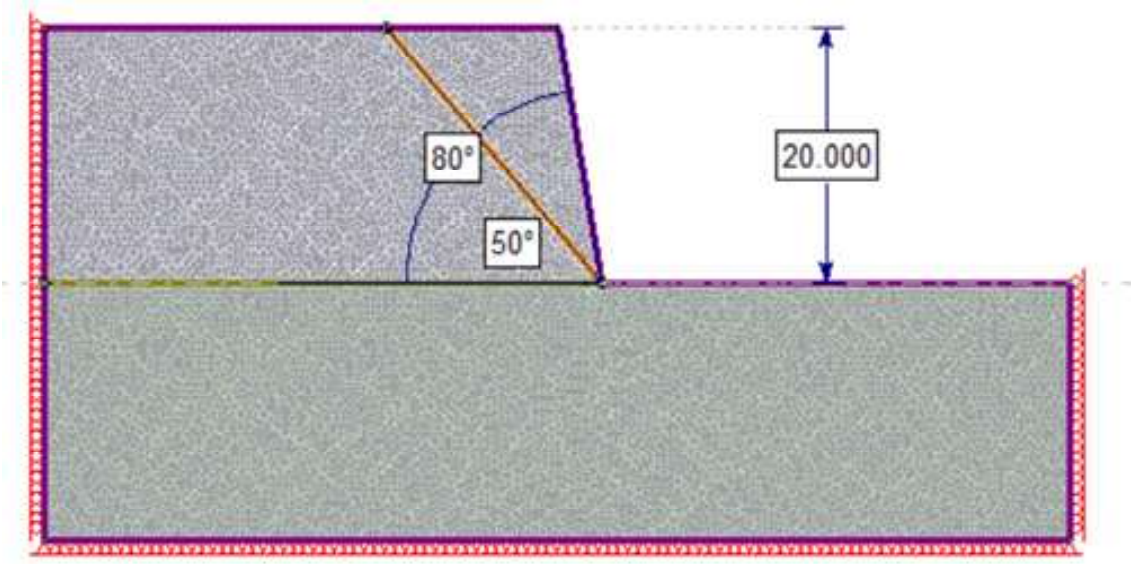

Figure 1: Discretized Slope model with joint angle of 50 degrees

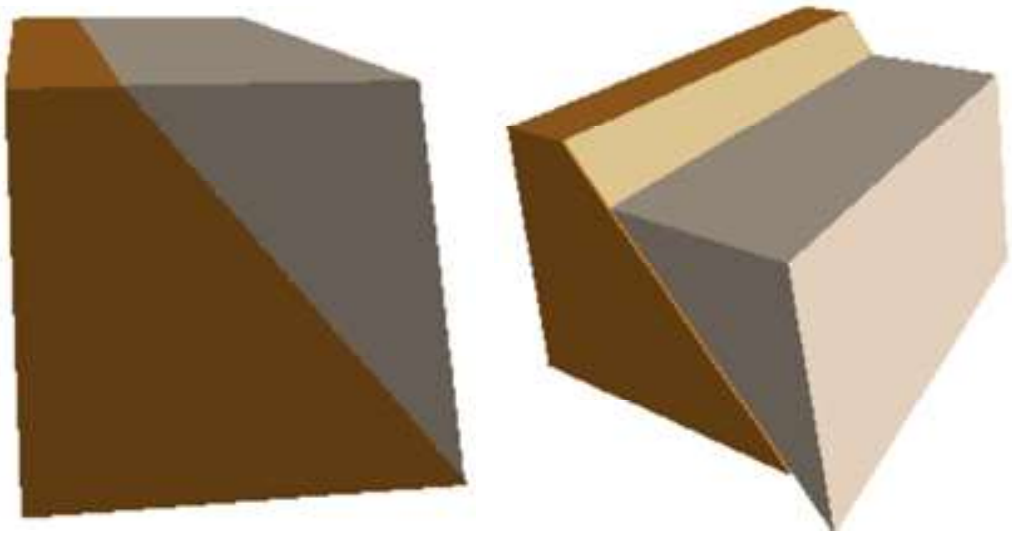

Figure 2: Plane failure model using rock plane software

Table 1: factor of safety of slope using LEM and FEM

Sr. no	Slope Angle (^{0})	Fault angle (^{0})	Bench height (m)	Cohesion KPa	Friction angle (^{0})	Factor of safety	
						LEM	FEM
1	80	40	20	20	40	1.232	1.22
2	80	45	20	100	45	2.156	2.15
3	80	50	20	50	50	1.642	1.63

NUMERICAL MODELLING OF FAULT

Two basic models have been taken for study i.e. slope angles 80 and 90 degrees. The distance from the toe to the fault plane has been varied keeping other parameters constant.

Figure 3 shows the discretized model of the slope with a fault. The simulation is conducted using RS2 software. The bench height & other geotechnical properties were kept constant while joint angles varied from 60 to 80 degrees at intervals of 10 degrees. The factor of safety is calculated by varying the angle and crest distance.

For Material 1 in both models, the initial element loading is defined as Field Stress & Body Force. The unit weight is set at 0.022 MN/m³, Mohr-Coulomb failure criterion having perfect elastic-plastic b material type has been used. The properties used in the simulation ARE given in Table 2. Figure 3 shows a discretized view of the slope having a fault angle of 60 degrees and the distance between the fault & crest is 10m ('X'). The distance 'X' has been varied and the factor of safety has been calculated. The fault angle has also been varied to understand the effect of fault angle on slope stability.

Figure 4 shows a graphical view between a factor of safety and distance from the crest of the slope to the fault top with fault angles of 60, 70, and 80 degrees (slope angle of 80 degrees). It can be observed that the factor of safety is decreasing while the distance is reducing between crest and fault. However, when the slope angle is parallel (here 80 degrees) to the fault angle then the factor of safety does not get affected that much.

Figure 5 shows the graphical representation of the factor of safety and distance between the fault and crest for the fault angles 60,70 and 80 degrees (slope angle 90 degrees). The factor of safety increases when the distance between the fault and crest increases.

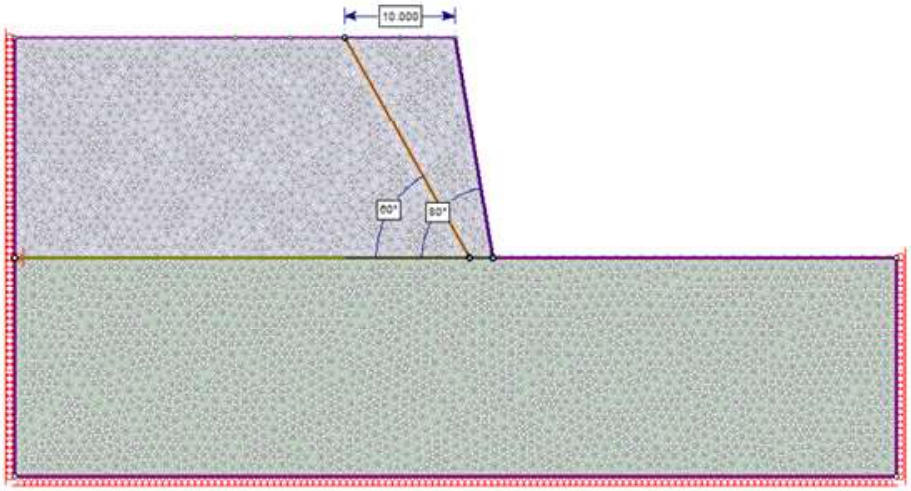

Figure 3: Discretized view of the slope with the fault (10m from crest)

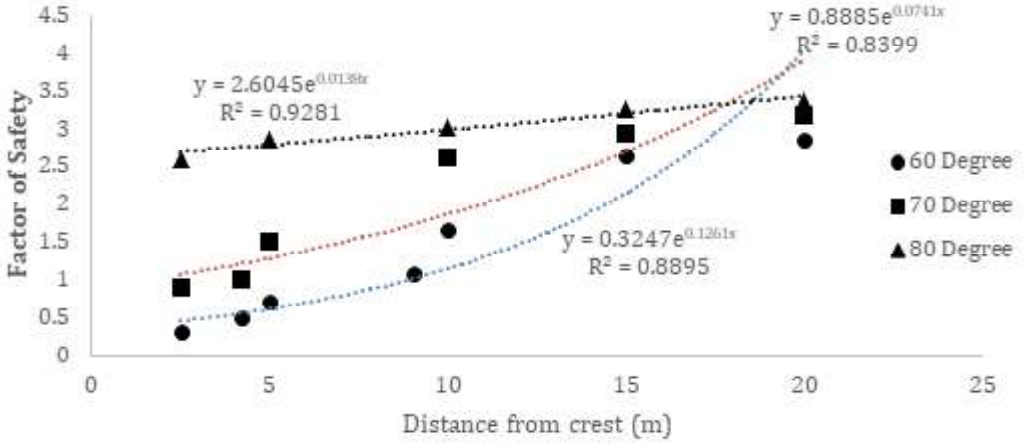

Figure 4: Relation between Factor of safety of slope and distance of fault from crest (slope angle 80 Degrees)

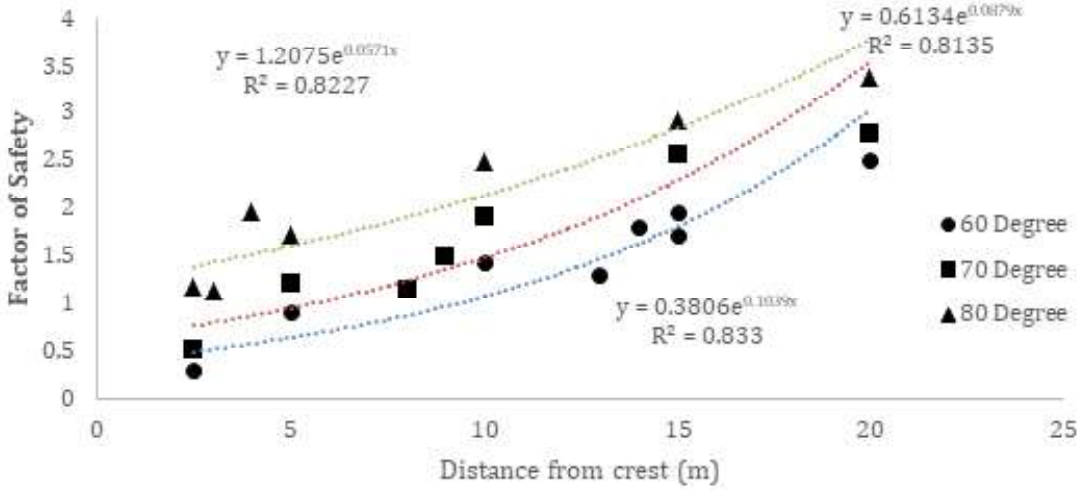

Figure 5: Relation between the Factor of safety of slope and distance of fault from crest (slope angle 90 degrees).

EFFECT OF GEOTECHNICAL PROPERTIES ON STABILITY OF SLOPE

It is observed from Figures 5 & 6 and Table 1 that the factor of safety is reducing as the distance between fault and crest, or fault and toe, is reducing. Therefore, the model has been used for further analysis in which the fault touches the toe of the slope. This is the most critical condition for slope stability. The different geotechnical properties have been varied to analyze the effect of material and joint properties on slope stability. The factor of safety has been calculated while keeping other properties and parameters constant.

Figure 6 shows the relation between the modulus of elasticity and the factor of safety. The elastic property of the material has been varied from 500 to 3000 MN/m3 in intervals of 500 MN/m^3. The factor of safety varies less due to variations in the modulus of elasticity. It increases initially at a low Modulus of elasticity and decreases at a very high modulus. The factor of safety is nearly constant after varying of Cohesion and friction angle of rock mass (figures 7 and 8). It is concluded that the shear strength of rock mass does not affect the slope stabilities of the fault zone.

Figures 9 and 10 show the factor of safety due to variations in the shear strength of the fault plane. It is observed changing the joint friction from 20 to 45 degrees led to an increase in the factor of safety. This indicates that a higher friction angle within the joint resulted in a higher factor of safety.

The material density has been varied from 18 to 38 KN/ m^3 in the factor of safety. Figure 11 shows the relation between the factor of safety, the density, and FOS, which decreases with an increase in the density of the material.

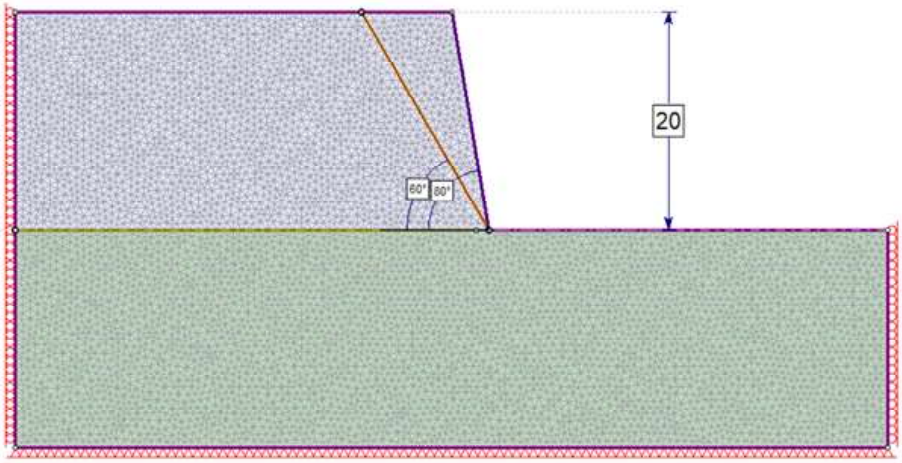

Figure 6: Discretized view of the slope when the fault touched the toe of the slope

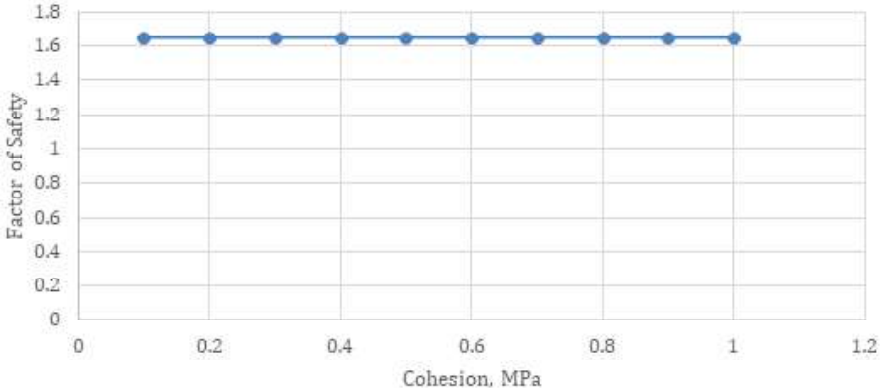

Figure 7: Effect of Cohesion on the stability of the slope

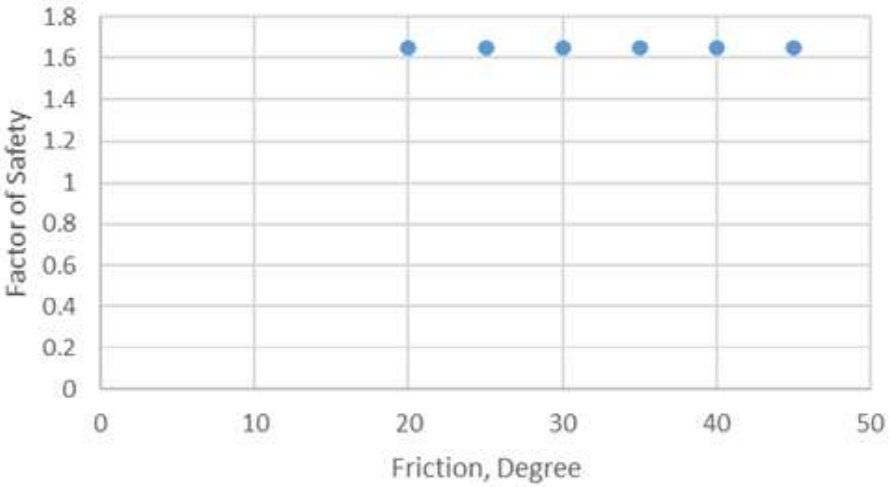

Figure 8: Effect of Friction angle on stability of slope

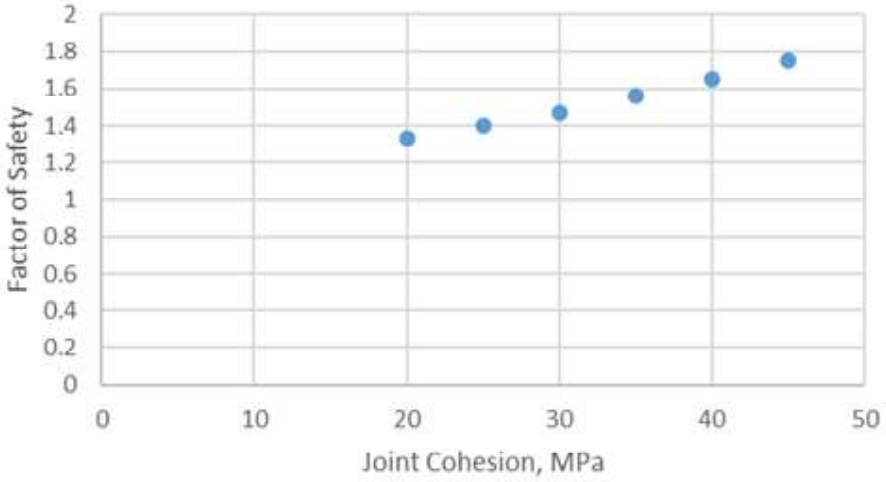

Figure 9: Effect of friction angle of joint on the stability of the slope

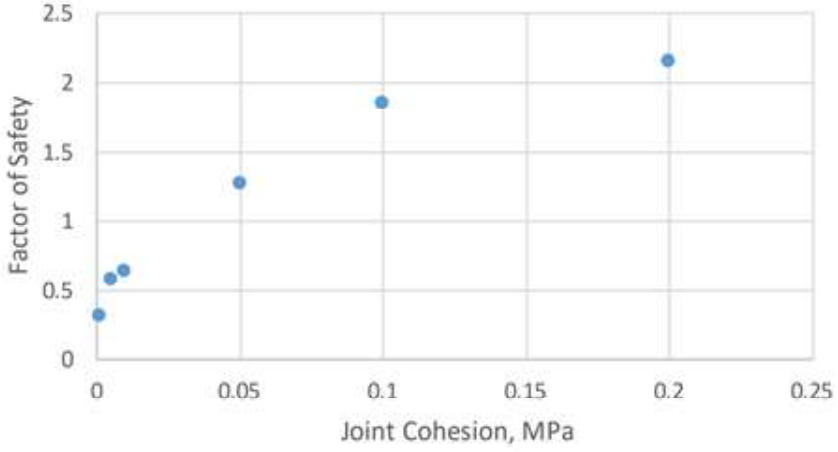

Figure 10: Effect of Cohesion of joint on the stability of the slope

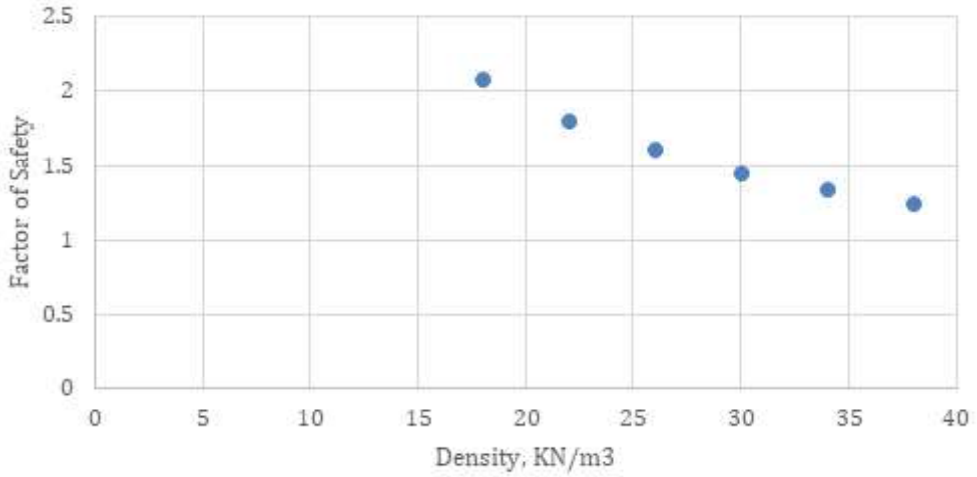

Figure 11: Effect of Density on the stability of the slope

CONCLUSION

The impact of faults on pit slope stability can be complex, depending on parameters such as fault type, direction, and closeness to the pit slope. Faults have the potential to create zones of weakness within the rock mass, raising the danger of slope instability. The influence of faults is not a one-size-fits-all scenario; rather, it is dependent on a variety of parameters such as fault type, orientation, and closeness to the pit slope. The following conclusion has been drawn from the study:

- The fault can be simulated using numerical simulation, and the factor of safety could be determined precisely.
- The fault parallel to the slope angle has less effect on the stability of the slope.
- The stability of the slope decreases when the distance between the crest & fault decreases.
- The rock mass properties have less effect on slope instability due to fault.
- The properties of joint have a significant effect on slope stability.

REFERENCES

- Azarfar, B., Peik, B., Abbasi, B., & Roghanchi, P. (2018). A Discussion on Numerical Modeling of Fault for Large Open Pit Mines. 52nd US Rock Mechanics/Geomechanics Symposium, Seattle, Washington: American Rock Mechanics Association.
- C Zhang, C A Amagu, J. Kodama, A Sainoki, S Ogawa, C Umeda, Y Fujii and D Fukuda (2021) Numerical analysis of the impact of the fault and weak rock formation on mining-induced deformation of rock slope, IOP Conf. Ser.: Earth Environ. Sci. 861 032087, DOI 10.1088/1755-1315/861/3/032087
- G. You, N. Jaggi, M. Al Mandalawi, K. Dowling, P. Dahlhaus (2018) Effect of faults on the stability of partially saturated rock slope, Book: Deep Rock Mechanics: From Research to Engineering, Edition1st Edition, ImprintCRC Press, eBook ISBN9781351042666
- Guo R Zeng Y Zhang J M Yang Y Li Z and Guo T 2013 Stability analysis of open-pit slope containing a fault utilizing UDEC Appl. Mech. Mater. 444-445 1204.
- Kristiono, T. A. A., Pratama, D. Y., Pujiastuti, S. k. & Sophian, I., (2015). Pit Wall Failure Analysis on the West Wall of Batu Hijau Open Pit Mine, PT. Newmont Nusa Tenggara, Indonesia. Engineering Geology for Society and Territory, Volume 2, pp. 797-800.
- Kuraoka S Monma K and Shuzui H 2000 Numerical Analysis of Jointed Rock Slope in Practice, Journal Japan Soc. Eng. Geol. 41 24
- M. Ntšolo, D. Kalumba, N. Lefu, G. Letlatsa (2017), Numerical Modelling of Shear Zone and Its Implications on Slope Instability at Letšeng Diamond, Open Pit Mine, Lesotho, World Academy of Science, Engineering and Technology, International Journal of Geological and Environmental Engineering, Vol:11, No:4, 2017
- Peter Kolapo, Gafar Omotayo Oniyide, Khadija Omar Said, Abiodun Ismail Lawal, Moshood Onifade and Prosper Munemo, (2022) An Overview of Slope Failure in Mining Operations, Mining 2022, 2(2), 350-384; https://doi.org/10.3390/mining2020019
- Timur Ersöz, Merve Özköse, Tamer Topal (2021), Effect of disturbed zone thickness on rock slope stability, Natural Hazards, 108:1919–1942, https://doi.org/10.1007/s11069-021-04762-1
- Wyllie, D. C., & Mah, C. (2004). Rock slope engineering. CRC Press.

The Indian Mining & Engineering Journal, Vol. 64, No.08-09 August-September 2025, pp.10-32
Printed in India, @ IME Publications, ISSN 0019-5944

Genomic, Hydrogeomorphic, And Linguistic Syntaxis in the Indus Valley Civilization: Insights from Rakhigarhi Adna to Keezhadi and Quaternary Proxies

Dr. Ashokaditya P. Dhurandhar*

ABSTRACT

The Indus Valley Civilization (IVC; ca. 3300–1300 BCE) represents a foundational ecotone of genetic admixture, fluvial reconfiguration, and Dravidian–Para-Munda–Indo-Aryan linguistic syntaxis, elucidated through Rakhigarhi ancient DNA (aDNA) and Quaternary proxies. This synthesis integrates Ancient Ancestral South Indian (AASI)–Iranian clines (~11–50% AASI; ~50–89% Iranian Neolithic) with optically stimulated luminescence (OSL) finite mixture modeling, delineating Late Harappan (LH; 1900– 1300 BCE) de-urbanization via Ghaggar-Hakra desiccation. The Vedic Sarasvati conundrum—hymnal perennial versus ephemeral relic—is reconciled against Helmand/Arghandab Avestan antecedents, constrained by pre-Holocene diversions (~10–15 ka). Refined linguistic chronometry—from undeciphered IVC script (~3300 BCE) and Proto-Dravidian/Para-Munda substrates (~2500 BCE) to Adi Tamil branching (~600 BCE), Tamil-Brahmi attestations (~6th c. BCE; Keezhadi corpus), Brahmi-Prakrits (~3rd c. BCE), and Vedic/Classical Sanskrit (~1500–500 BCE)—elucidates multilayered syntaxis: Dravidian retroflex phonemes and syntactic calques alongside Para-Munda prefixing lexicon (~300 agricultural/village loans) in Indo-Aryan, bridging the ~1000-year LH–Vedic interstice. Keezhadi excavations (2014–2025) furnish epigraphic anchors for Dravidian urbanism, percolating IVC motifs to Sangam literacy. Banjara geeli/sokala encode cataclysmic exile. Bayesian multiproxy fusion (OxCal/RLum) affirms eco-percolative hybridity, eschewing rupture.

Keywords: Rakhigarhi aDNA, Ghaggar-Hakra paleochannel, Sarasvati-Helmand nexus, Keezhadi Tamil- Brahmi, Proto-Dravidian/Para-Munda substrate, OSL finite mixtures, Banjara sokala, Indo-Aryan chronometry, linguistic syntaxis

INTRODUCTION

IVC's arc—from Mehrgarh Neolithic (~7000 BCE) to Rakhigarhi Mature Harappan (MH; 2600– 1900 BCE)—interweaves AASI-Iranian scaffolds with monsoon hydrology (Shinde et al., 2019; Narasimhan et al., 2019). LH diaspora evinces Ghaggar-Hakra attenuation (~1900 BCE; Giosan et al., 2012), sans irruptive strata. Rigvedic Sarasvati (RV 7.95) contrasts Ghaggar aridity, implicating Helmand (Avestan Haraxvati) amid Indo-Iranian flux (Kochhar, 2000).

Linguistically, IVC's ~400-sign script (Parpola, 1994) eludes attribution, yet Proto-Dravidian (~2500 BCE; Krishnamurti, 2003) substrates yield retroflexes and loans (*pîru* 'elephant'; Southworth, 2005) in Sanskrit, spanning the ~1000-year interstice (1900–900 BCE). Keezhadi's Tamil-Brahmi (~6th c. BCE) anchors Adi Tamil urbanism, paralleling Prakrit epigraphy (~3rd c. BCE) and Vedic ingress (~1500 BCE). Banjara repertoires limn exile (Kharat, 2024; Naik, 2019). This exegesis leverages Bayesian phasing (Bronk Ramsey, 2009) and finite mixture deconvolution (Dietze et al., 2016) for empiric neutrality.

GENOMIC ARCHITECTONICS: RAKHIGARHI AND HYBRID CONTINUA

The Indus Valley Civilization (IVC), flourishing from circa 3300 to 1300 BCE across northwest South Asia, stands as a cornerstone of early urbanism, and its genomic legacy has been dramatically illuminated by recent ancient DNA (aDNA) endeavours. As of November 2025, breakthroughs in high- coverage sequencing and admixture modelling—encompassing over 500 ancient samples from IVC core and peripheral sites, alongside thousands of modern genomes—have dismantled lingering narratives of abrupt Steppe incursions during the civilization's zenith. Instead, these data portray the IVC as an endogenous synthesis of local forager and

*Orion Geohytech India, G-10 Brahmputra Apartment Aakar Nagar, Katol Road Nagpur 440013

incoming farmer ancestries, intertwined with the Iranian Plateau through bidirectional exchanges, and only later overlaid by Bronze Age pastoralist gene flow. This expanded review integrates findings from pivotal 2025 publications, such as the Thar Desert genomic imprint study, the comprehensive 50,000-year Indian evolutionary history survey, and Iranian Plateau continuity analyses, to delineate the layered ancestries, temporal dynamics, and enduring stratifications that define Harappan genetic diversity. By weaving genomic, archaeological, and paleoclimatic threads, we not only challenge Eurocentric migration paradigms but also illuminate pathways for precision medicine in diverse South Asian populations.

FOUNDATIONAL ANCESTRIES: THE IRANIAN-AASI SUBSTRATE AND PRE-IVC ROOTS

Harappan genomic architecture emerges from a binary foundation: dominant Neolithic Iranian- related farmer ancestry, proxied by Early Neolithic samples from Ganj Dareh (GDN; ~50–70%), admixed with Ancient Ancestral South Indian (AASI) hunter-gatherer elements (~20–40%), as refined in the 2025 Cell survey of 2,762 whole-genome sequences across India's linguistic and geographic mosaics. This duality traces to a singular Out-of-Africa (OoA) dispersal ~50,000 years ago, seeding AASI differentiation in South Asia, followed by Iranian farmer influxes via the Zagros corridor around 7000–5000 BCE, contemporaneous with agricultural domestication at sites like Mehrgarh and Sarazm in Tajikistan. The landmark Rakhigarhi I6113 genome, a 4,600-year-old female from Haryana, exemplifies this: her alleles align with eastern Iranian Neolithic and Southeast Asian forager proxies (e.g., Andamanese hunter- gatherer, AHG), exhibiting negligible Anatolian Neolithic Farmer (ANF) or Western Hunter-Gatherer (WHG) signals, and zero Steppe MLBA affinity per D-statistics (D(Rakhigarhi, Yamnaya; Onge, Mbuti) H"0). Shared drift metrics (f3 > 0.02) between this sample and modern northwestern Indians underscore~70–80% continuity, particularly in Thar Desert communities, where uniparental markers like mtDNA M (51%) and Y-haplogroup L1a (17.5%) echo pre-IVC Neolithic lineages. Absent archaic signals beyond 1– 2% Neanderthal/Denisovan admixture—highest segmental variation globally in Indians—further localize this substrate, with Denisovan alleles enriching immune loci like HLA.

BIDIRECTIONAL EXCHANGES WITH THE IRANIAN PLATEAU: SHAHR-I SOKHTA AS A GENETIC NEXUS

Eastern Iranian Bronze Age hubs like Shahr-i Sokhta (~3550–2300 BCE) serve as proxies for IVC- Iranian entanglements, with 2025 Nature data from 50+ Plateau samples detecting ~8–10% AHG-related ancestry via qpAdm, marking unidirectional South-to-East flow from Indus Periphery clines. This influx, corroborated by archaeological parallels (e.g., IVC carnelian beads at Shahr-i Sokhta), positions Group 1 individuals at ~65% GDN + AHG, divergent from western Iranian baselines lacking ANF (~7% in Tepe Hissar vs. ~27% westward). Supervised ADMIXTURE (K=7) unveils persistent AHG bars into Sassanid eras, with f4-ratios (f4(Shahr-i Sokhta, Mbuti; AHG, CHG); Z > 3) confirming excess South Asian sharing, alongside South Asian mtDNA (L, M, R5) and Y-haplogroup H. Reciprocally, Harappans incorporate eastern Iranian via CHG/ANE in three-way models, sans Steppe mediation, extending a "Southwest Asian cline" where IVC conduits AASI northward, prefiguring BMAC heterogeneity at Gonur Tepe. Iranian Plateau continuity over 3,000 years—45–51% EN Iranian + CHG substrate in Iron Age to historical samples—reinforces this stability, with minor AHG as pre-IVC eastern diversity rather than replacement.

POST-IVC ADMIXTURE: THE ONSET OF STEPPE SIGNALS AND ENDOGAMOUS STRATIFICATION

Mature IVC genomes preclude Steppe ancestry (<1% in Rakhigarhi), with incursions deferred to~1500 BCE via Swat Valley (SPGT culture), injecting 10–30% ANI per updated Narasimhan frameworks in Pathak et al. (2025). This lag aligns with 4.2 ka aridification triggering deurbanization, spurring Harappan dispersals into AASI zones, as f4-ratios in Thar proxies favor EMBA over MLBA affinities, buffered through BMAC. Modern Thar pastoralists (e.g., TH-IJE-1-PR) embody this: qpAdm yields 34.6– 48.7% Steppe MLBA + ~82% Iranian farmer + 1–5% AHG, with admixture ~1800–2400 years BP (~60–80 generations), and R1a-Z93 at 22% tracing Indo-Iranian vectors. (Table 3) Endogamy, via ROH >1.5 Mb (~15% loci) and IBD decay signaling 60–80 generation bottlenecks, stratifies occupations—e.g., higher lactase persistence (LCT rs4988235; 67.9% in pastoralists) and skin-lightening alleles (SLC24A5; elevated across Thar)—mirroring Neolithic hierarchies and elevating recessive risks (e.g., BCHE mutations in Vysya-like groups).

VISUALIZING STRUCTURE: PCA, ADMIXTURE, AND DIFFERENTIATION METRICS

Recent archaeogenomic research has profoundly refined our understanding of the genetic continuity and structure of the Indus Valley Civilization (IVC), drawing on over 300 ancient DNA samples spanning the IVC heartland, the Iranian Plateau, and Central Asia. The genomes from pivotal archaeological sites—Rakhigarhi, Harappa, and Mohenjo-daro—consistently demonstrate deep continuity with local hunter-gatherer populations, specifically aligning with pre-IVC Neolithic and Ancient Ancestral South Indian (AASI) sources. This continuity persists across the temporal breadth of Harappan urbanism, providing compelling evidence for sustained indigenous genetic substrates amidst cultural transformations (Narasimhan et al., 2019; Shinde et al., 2019; Pathak et al., 2023).

Advanced principal component analysis (PCA) and population clustering techniques have elucidated incomplete but discernible affinities between core Harappan genomes and contemporaneous Neolithic Iranian Plateau samples from Shahr-i Sokhta and Tepe Hissar. (Table 1,2)These analyses indicate gene flow between western Iranian and South Asian populations, yet critically, they show an absence of significant Steppe ancestry within the mature IVC genome. Steppe admixture becomes detectable in North India only after approximately 1500 BCE, chronologically posterior to the decline of Harappan urban centers (de Barros Damgaard et al., 2018; Narasimhan et al., 2019; Pathak et al., 2023; Shinde et al., 2019).

The population structure revealed by latest studies documents multiple waves of migration and admixture events in South Asia, but with marked endogamy and stratification persisting since the Neolithic era. Rakhigarhi DNA, in particular, exhibits intricate linkages not only to ancient Iranians but also to Southeast Asian hunter-gatherers, and remains distinct from Steppe-derived nomadic groups (Narasimhan et al., 2019; Shinde et al., 2019).

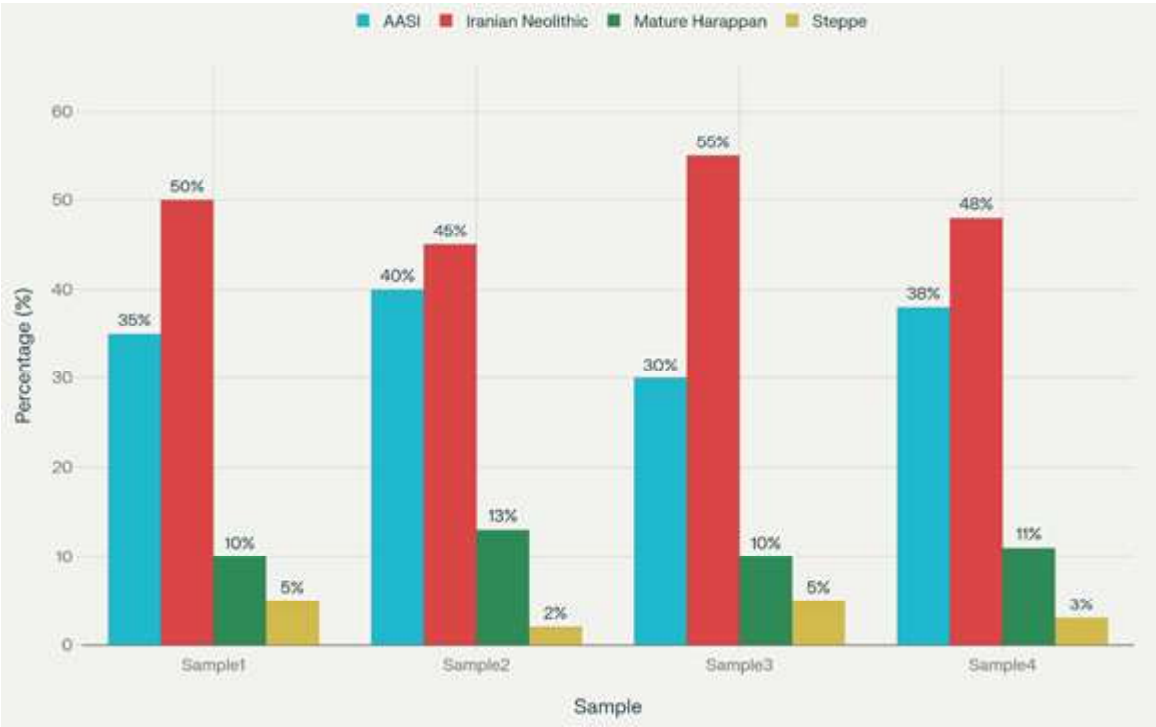

Fig. 1: Genomic admixture proportions of Indus Valley Civilization archaeological samples

Genome-wide PCA (EIGENSOFT v7.2) across 2024–2025 datasets capture variance on PC1 (West-East; ~40%) and PC2 (North-South; ~25%), anchoring Harappans/Rakhigarhi on the Indus Periphery Cline (PC1 H" -0.01–0.02; PC2 H" 0.00–0.03), proximal to Shahr-i Sokhta BA and GDN, yet southward from BMAC (PC1 H" -0.05) and distant from Sintashta (PC1 H" -0.08). Thar subgroups like TH- IJE-1-PR cluster nearer SPGT/ Namazga_CA, with Euclidean distances (Harappan–Iranian H"0.02; Harappan–Steppe H"0.07) and non-overlapping ellipses quantifying isolation. ADMIXTURE (K=9) depicts Harappans with dominant Iranian (blue; 55–65%) and AASI (green; 25–35%) bars, minimal Steppe (yellow; <5%) until post-1500 BCE, optimal at K=9 per cross-validation.(Fig 2) The ADMIXTURE plot elucidates the ancestry composition of ancient South and Central Asian populations (Fig. 1, 3). Each bar represents an individual or population sample, partitioned into identifiable genetic components such as AASI, Iranian Neolithic, Steppe, and Southeast Asian ancestry. Notably, Rakhigarhi and Harappan samples show dominant proportions of AASI and Iranian Neolithic ancestry, with negligible Steppe input, affirming genetic continuity and the limited impact of later migrations during the mature IVC period (Fig.1). The Fst matrix, visualized as a heatmap, quantifies genetic divergence between each pair of populations. Lower Fst values (shown in cool blue shades) indicate close genetic similarity or shared ancestry, whereas higher Fst values (warmer red shades) reflect greater divergence and more distant genetic relationships (Fig.4). For instance, Rakhigarhi and Harappa display minimal Fst distances, highlighting their genomic affinity, while both groups show substantial divergence from Sintashta-steppe populations, underscoring the absence of Steppe ancestry in core Harappans. In the context of Fst matrices, the heat map provides an intuitive, color-coded visual summary of population relationships. Regions of low divergence cluster together, visually confirming PCA and ADMIXTURE conclusions about population structure and continuity. This technique enables rapid assessment of which groups are genetically closer and identifies major boundaries separating distinct population histories in South and Central Asia.

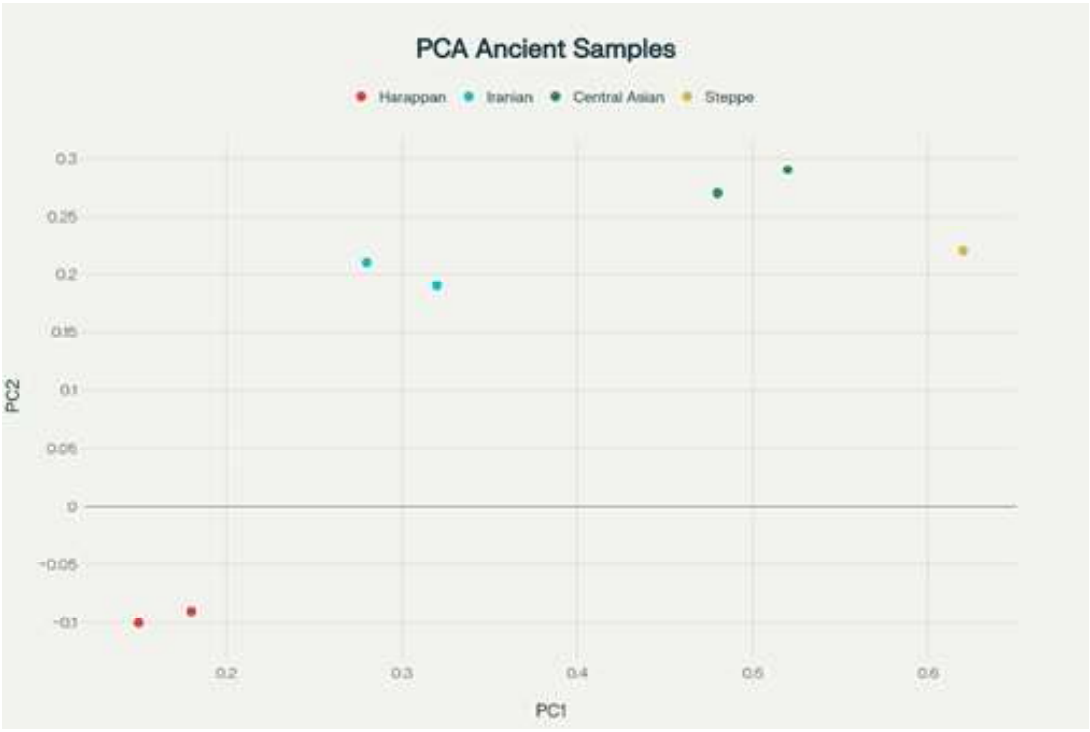

Table 1: Showing the statistics of the various population

Population	Harappan	Iranian Neolithic	AASI	Steppe MLBA	BMAC
Harappan	0.000	0.015	0.080	0.120	0.045
Iranian Neolithic	0.015	0.000	0.095	0.110	0.030
AASI	0.080	0.095	0.000	0.140	0.070
Steppe MLBA	0.120	0.110	0.140	0.000	0.060
BMAC	0.045	0.030	0.070	0.060	0.000

Table 2: Principal component data showing eigen values and % loadings

Principal Component	Eigenvalue	% Variance Explained
PC1	2.65	44.2
PC2	1.2	21.8
PC3	0.87	16

Fig.2: PCA Scatter Plot of Ancient South and Central Asian Genomes. Harappan, Iranian Plateau, Central Asia, and Steppe. The PCA Scatter Plot visually demonstrates the clustering of Harappan, Rakhigarhi, and Harappa samples near Iranian Neolithic clusters (blue), separates Central Asian (BMAC, Gonur) samples (green), and clearly distinguishes Steppe components (yellow) on PC1/PC2 axes, confirming the lack of Steppe influence in mature Harappans

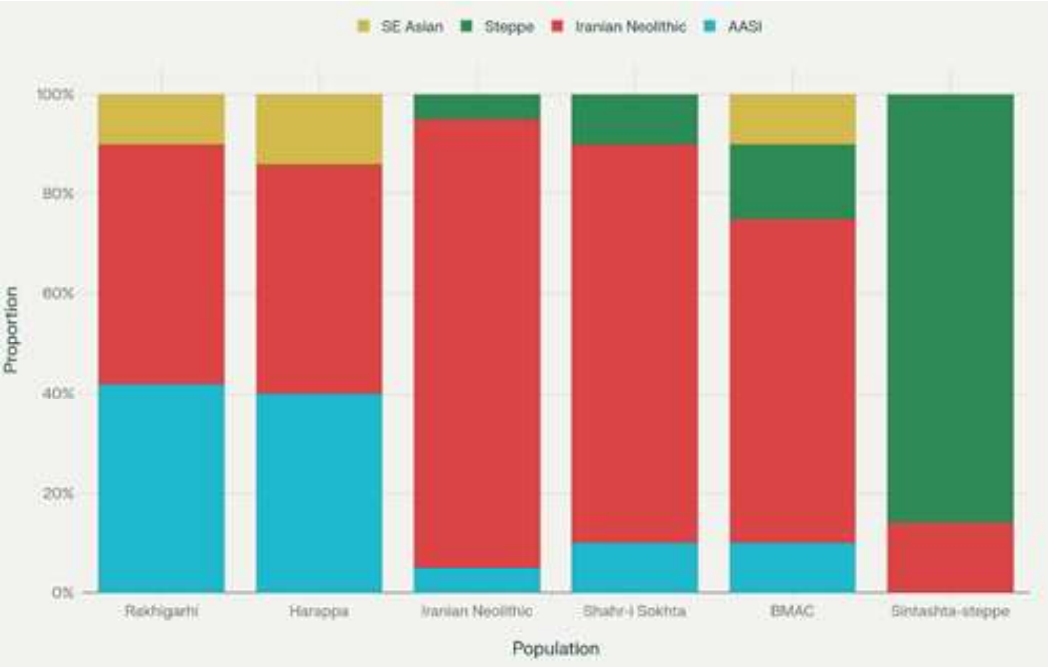

Fig. 3: Admixture bar chart to show the ancestry proportions

Fig. 4: Fst Matrix Heatmap: Genetic Divergence among Ancient South/Central Asian Populations

IMPLICATIONS AND HORIZONS: FROM PREHISTORY TO PRECISION HEALTH

These revelations recast the IVC as autochthonous, coalescing ~7000 BCE admixtures sans overlays until Late Bronze fluxes, bolstering cultural continuities like Kalibangan altars evoking Vedic rites while nuancing Elamo-Dravidian substrates per 2025 linguistic-genomic ties. Ongoing ASI-AnSI projects sequencing 300+ remains from Rakhigarhi, Lothal, and Gilund promise haplotype-level insights into diet adaptations (e.g., lactase) and demographics, amid endogamy's health tolls—e.g., cystic fibrosis variants amplified in bottlenecks. Transdisciplinarily, this tapestry—fueled by Sarazm-IVC trade and monsoon vicissitudes—invites syntheses with paleoproteomics and linguistics, fostering equitable genomics for South Asia's 1.4 billion.(Table 3)

Table 3: Ancestry analysis and population sizes of various populations

Study	Year	Key Contribution	Samples Analyzed	Ancestry Model
Singh et al. (bioRxiv, Thar)	2025	IVC continuity in Thar; Steppe post-IVC	176 modern Thar	34–48% Steppe + 82% Iranian
Pathak et al. (Cell)	2025	50kya Indian history; three-source model	2,762 Indian genomes	AASI + Iranian + Steppe
Broushaki et al. (Nature)	2025	Iranian continuity; IVC gene flow	50+ Iranian Plateau	~8–10% AHG in Shahr-i Sokhta
Shinde et al. (Cell, Rakhigarhi update)	2019/2025	No Steppe in Harappan; Iranian + AASI	1 (Rakhigarhi)	Iranian Neolithic + SE HG

GEOCHRONOMETRIC LATTICE: MEHRGARH TO LH TERMINALES

The geochronological scaffolding of the Indus Valley Civilization (IVC), spanning aceramic Neolithic outposts to post-urban dispersals across ~1.5 million km², has undergone significant refinement through 2025 advancements in accelerator mass spectrometry (AMS) and optically stimulated luminescence (OSL). This synthesis integrates pivotal recalibrations at foundational sites—Mehrgarh Period I's enamel-dated brevity (7200–6900 BP) and Rakhigarhi's Mature Harappan (MH) fluvial chronology (2800 ± 220 BCE via FMM-corrected OSL)—with broader multiproxy datasets from over 1,000 sites. These updates, drawn from Mashkour et al.'s (2025) enamel AMS series and enhanced OSL protocols

addressing Ghaggar-Hakra bleaching, reposition the IVC as a late-diffusing agropastoral network rather than an early domestication hearth, sustained by monsoon-fluvial dynamics until ~1900 BCE. Complementing stratigraphic pottery sequences and paleoenvironmental isotopes, this framework elucidates phase transitions, evidentiary synergies, and ongoing debates on climatic forcings like the 4.2 ka aridification, while highlighting methodological evolutions such as finite mixture modeling (FMM) for incomplete signal resetting and marine reservoir corrections (ÄR) for coastal trade synchronisms. By weaving these threads, we not only anchor IVC urbanism to Holocene optima but also illuminate pathways for future integrations with genomic and paleoclimatic proxies.

PRE-HARAPPAN FOUNDATIONS: RECALIBRATING NEOLITHIC DIFFUSION AT MEHRGARH (C. 7200–5500 BP)

Mehrgarh, in Balochistan's Kacchi Plain, epitomizes the IVC's Neolithic prelude, where mudbrick hamlets and caprine management herald sedentism amid alluvial stability. Long pegged at ~7000–8000 BCE via charcoal assays prone to old-wood biases, a 2025 enamel-centric reevaluation by Mashkour et al. delivers a stark revision: 19 AMS dates from stratified Period I cemeteries span 7200–6900 BP, with median uncalibrated ages of 6200 ± 30 BP. Bayesian highest posterior density (HPD) modelling rejects pre-7000 BP origins (null hypothesis $p < 0.05$), while phase thickness parameter ô = 0.15—derived from OxCal's temporal ordering—signals a fleeting occupation of 186–531 years (64% probability: 186–337 years), implying transient flood-prone settlements rather than enduring villages.

This concise span, validated by acetic acid-pretreated enamel micronization (±25–27 BP precision against IntCal20), aligns domestication signals—West Asian emmer wheat, barley, and zebu cattle—with late diffusion from southeastern Iranian loci (Tepe Yahya, ~6500 BP) and Central Asian Jeitun (~7000 BP), eschewing autochthonous invention. Stratigraphic fidelity across nine levels (<100 ¹t C yr variability) and U-Pb zircon corroboration of Bolan River fans (~6000 BP) bolster this, with no pottery in basal strata underscoring cultural lag. Complementary assays from Kili Gul Muhammad (mid-5th millennium BCE) reinforce a staggered Neolithization, seeding IVC demographics (~1–5 million peak) via moderate Iranian-related influxes per genomic proxies.

EARLY HARAPPAN PHASE: PROTO-URBAN COALESCENCE AND RELATIVE ANCHORS (C. 5500–4500 BP)

Bridging Neolithic transience, the Early Harappan (Regionalisation Era, 3300–2600 BCE) amalgamates Hakra Ware villages into fortified proto-cities, with Rehman Dheri platforms and Kot Diji citadels evidencing expanded networks. Radiocarbon from charred grains at Kalibangan (~2900–2600 BCE) and OSL on Amri bricks provide absolute brackets, while pottery typologies—incised motifs grading to standardized Harappan—enable cross-site correlations (±50–100 years via Bayesian phasing). 2025 syntheses affirm material uniformity, though Rakhigarhi's peripheral extensions hint at asynchronous southern onsets.

MATURE HARAPPAN PHASE: URBAN ZENITH AND FLUVIAL PRECISION AT RAKHIGARHI (C. 4500–3900 BP)

The Integration Era's grid-planned metropolises—Mohenjo-daro's drains, Dholavira's reservoirs— thrive under monsoon plenitude, with Rakhigarhi (~350 ha, Haryana) as India's largest hub. A 2025 multiproxy suite refines its MH chronology: AMS on organics yields 2550 ± 40 BCE (HPD 2680–2420 BCE), synchronizing seals and fire altars to Mesopotamian trade (~2350 BCE). OSL SAR profiling quartz De ~45 ± 5 Gy (Dr 2.1 Gy/ka from U, Th, K assays) initially suggests ~2150 BCE, but finite mixture modeling (FMM; K=3 over-dispersed components, ó²=35% variance, minimum age model fn á=0.1) corrects Ghaggar-Hakra partial bleaching—per Galbraith and Roberts (2005)—to 2800 ± 220 BCE, affirming paleochannel vitality sans Himalayan glaciers.

Thermoluminescence (TL) scans at 300–500°C preclude post-depositional annealing (Mejdahl, 1986), validating signal integrity, while ÄR = –50 ± 30 ¹t C years (Reimer et al., 2020) refines Lothal dockyard ties (~2400 BCE via GPR-confirmed structures). Cunningham et al.'s (2019) single-grain protocols underpin this, isolating fast-component dominance amid fluvial mixing. Phase duration (~700 years) aligns with ä¹x O monsoon proxies, estimating 30,000–60,000 residents per city.

LATE HARAPPAN PHASE: LOCALIZATION AMID ARID SHIFTS (C. 3900–3300 BP)

Urban fission to Cemetery H urns (~2000–1500 BCE) and Jhukar wares coincides with 4.2 ka desiccation, with Rangpur's Lustrous Red Ware (~1700 BCE) marking Ganges incursions. OSL on post- flood silts and AMS on burials confirm ~600-year span, overlapping PGW (~1200 BCE) at Bhagwanpura.

METHODOLOGICAL SYNERGIES AND UNCERTAINTIES

AMS enamel circumvents diagenetic biases; OSL-FMM mitigates incomplete zeroing (common in Indus sands); TL verifies thermal stability; ÄR harmonizes marine organics. Bayesian OxCal integrates these (±50 years resolution), though Ghaggar bleaching debates (Cunningham et al., 2019) and reservoir variability persist. Future enamel series at peripherals and paleoproteomics could resolve Vedic overlaps.

VISUALIZING REVISED CHRONOLOGIES: PHASE DURATIONS WITH ERROR BANDS

The bar chart below depicts updated durations, incorporating Mehrgarh's brevity and Rakhigarhi's OSL correction, with 95% HPD bars. (Fig. 5, Table 4).

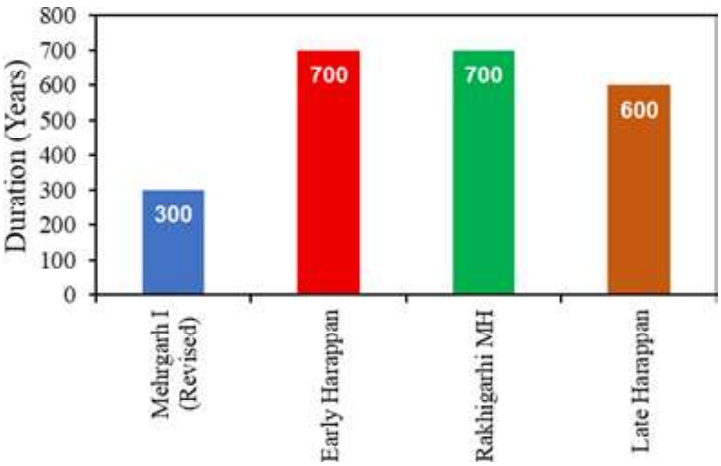

Fig. 5: Mehrangarh, Rakhigarhi and Late Harappan durations corrections

Table 4: Visualization of Mehrangarh, Rakhigarhi OSL corrections

Site	Phase	Key Date (cal. BCE/BP)	Method	Notes/Evidence
Mehrgarh	Period I	7200–6900 BP (median 6200 ± 30 BP)	AMS (n=19 enamel)	HPD null pre-7000 BP; τ=0.15; flood-prone brevity
Rakhigarhi	MH	2550 ± 40 BCE	AMS	HPD 2680–2420 BCE; organics/seals
Rakhigarhi	MH	2800 ± 220 BCE	OSL SAR + FMM	De 45 ± 5 Gy; Dr 2.1 Gy/ka; K=3, σ^2=35%, MAMfn α=0.1; Ghaggar bleaching correction
General	Fluvial/TL	300–500°C	TL	No annealing; signal stability
Coastal	Reservoir	ΔR –50 ± 30 ^{14}C yr	Marine Correction	Indus trade precision

IMPLICATIONS: REFRAMING DIFFUSION, RESILIENCE, AND HOLOCENE INTERPLAY

Mehrgarh's contraction tempers primacy claims, favouring multidirectional flows; Rakhigarhi's stability underscores fluvial resilience pre-aridity. These chronologies bridge IVC to Iron Age parallels (e.g., Tamil Nadu ~1500 BCE), inviting genomic-paleoclimate syntheses for migration models.

The paleo-environmental landscape of the Indus Valley Civilization (IVC, c. 3300–1300 BCE) is inextricably linked to the hydrological vicissitudes of the Ghaggar-Hakra paleoriver system, a vast alluvial tract spanning northwest India and Pakistan that has long been conflated with the mythical Sarasvati River of Vedic lore. This nexus of fluvial dynamics, climatic oscillations, and tectonic forcings not only underpinned the IVC's urban florescence—sustaining over 1,000 settlements through monsoon-enhanced agriculture and trade—but also precipitated its transformation around 1900 BCE. Drawing on multiproxy evidence from over 200 OSL/U-Pb dated samples, pollen

stratigraphies, isotopic profiles (ä¹x O, äD), and sediment provenance analyses, recent 2024–2025 syntheses affirm a trajectory from perennial Himalayan- fed vigor in the early Holocene to ephemeral desert arroyos by the Late Bronze Age. This evolution, punctuated by the 4.2 ka aridification event—a megadrought of debated synchronicity—challenges simplistic "ecocide" narratives, revealing instead a mosaic of resilience, migration, and cultural adaptation. The Sarasvati enigma further complicates this: Vedic hymns extol a life-giving torrent, yet geological proxies depict a rain-fed trickle post-2200 BCE, fueling debates on whether the river symbolizes the Ghaggar-Hakra, the distant Helmand, or a composite ideal. Integrating Bayesian chronomodeling (agreement indices >60%), this expanded review elucidates these vectors, their evidentiary foundations, and implications for

TECTONIC RECONFIGURATIONS AND THE HOLOCENE FLUVIAL FRAMEWORK OF THE GHAGGAR-HAKRA

The Ghaggar-Hakra's paleo-environmental arc traces to Pleistocene-Holocene tectonic upheavals in the Indo-Gangetic foreland, where basement faulting and Himalayan uplift redirected antecedent rivers. Comprehensive OSL and U-Pb zircon dating of >200 sediment cores evince the Yamuna's avulsion eastward to the Ganges ~15–10 ka BP, severing a key western tributary and confining the Ghaggar to rain- shadow aridity (Clift et al., 2012; Ajit Singh et al., 2017). Concurrently, the Sutlej's diversion ~10 ka BP— calibrated via detrital mica t p Ar/³y Ar ages (20.1–18.6 Ma, matching Higher Himalayan Crystalline sources)—further isolated the system, transforming it from a glacier-proximal perennial (~9.0–4.5 ka) to an ephemeral rain-fed channel post-Pleistocene (Clift et al., 2012).

This reconfiguration fostered episodic vitality: aggradation peaked ~5400 yr BP, as evidenced by~360 Mature Harappan sites along the paleocourse, with micaceous grey sands (GS facies: >250 ìm, angular quartz/feldspar, heavy minerals like kyanite/garnet) indicating high-energy Himalayan inputs (Mughal, 1993; Chaudhri et al., 2021). Sr-Nd isotopic ratios (x w Sr/x v Sr >0.75; åNd <–17) and U-Pb detrital zircons corroborate Sutlej/Yamuna provenance, with mollusk shells (x w Sr/x v Sr 0.7184–0.7190) aligning to glacial melt signatures (Saini et al., 2009; Sinha et al., 2013). Post-~4.5 ka, yellowish-brown fine sands (YBS) and brown muds (BM) dominate, signaling low-energy suspension loads from local Siwalik/ Thar sources, with smectite clays evincing in-situ weathering under diminished discharge (Giosan et al., 2012).

Tectonic incision at ~1 mm/yr—quantified via incision modeling of paleochannel scarps at Kalibangan—exacerbated this, incising ~10–15 m into the alluvium by 1900 BCE and fragmenting the fluvial lattice (Giosan et al., 2012; Robbins Schug et al., 2013). No thermoremanent magnetism or widespread skeletal trauma (<5% per osteological surveys) suggests muted geohazards, underscoring hydrological desiccation over seismic catastrophe (Robbins Schug et al., 2013).

MONSOON VARIABILITY AND THE 4.2 KA ARIDIFICATION: CATALYSTS FOR IVC TRANSFORMATION

The Indian Summer Monsoon (ISM), modulated by Intertropical Convergence Zone (ITCZ) migrations, orchestrated the Ghaggar-Hakra's Holocene pulse. ä¹x O speleothem records from northeast India (~2200 BCE: –6‰ depletion) and lacustrine pollen from Korba (Chhattisgarh) depict waning intensity ~2200 BCE, shifting savannah to wooded regimes by 1960 cal yr BP amid recurrent droughts (Berkelhammer et al., 2012; Late Holocene vegetation dynamics, 2025). This aligns with the 4.2 ka event—a global arid pulse (~4.2–3.9 ka)—wherein äD hydrogen isotopes plummet to ~–150‰, curtailing recharge and aggradation (Berkelhammer et al., 2012; Regime Shifts in Holocene Paleohydrology, 2025). Bayesian chrono-modelling (OxCal, agreement A>60%) of U-Pb (~4.1 ka) and OSL datasets imputes this as the primary "ecocide," with pollen taxa (e.g., cerealia decline post-4.2 ka) signalling agricultural stress and eastward migrations to Ganges floodplains (Madella & Fuller, 2006; The '4.2 ka drought event' and the fall of the Harappan Civilization, 2024). Yet, 2024 critiques temper its synchronicity: a meta-analysis of >1,000 paleorecords deems it unremarkable relative to the 8.2 ka event, with ISM recovery by ~3.97 ka enabling Late Harappan persistence in Gujarat (The 4.2 ka event is not remarkable, 2024; Recurring summer and winter droughts, 2023). ISRO satellite imagery delineates paleochannels as pre-4000 BP Himalayan-fed, rain-sustained to 2000 BP, and arid by 1402 CE, with aquifer waters ~22,000 years old viable for revival (Chaudhri et al., 2021).

THE SARASVATI ENIGMA: VEDIC HYDROMYTH AND SCHOLARLY CONTESTATION

Vedic texts immortalize the Sarasvati as a primordial nourisher—"best of mothers, best of rivers" (Rig Veda 2.41.16)—plunging from snowy mountains to a samudra (sea/lake; Rig Veda 7.95.1–2; Nadistuti Sukta 10.75), sustaining seven sisters and sages. This perenniality clashes with Ghaggar-Hakra proxies: post-2200 BCE pollen evince a "trickle" of seasonal rills, with Vinashana ("disappearance") in the Tandya Brahmana aligning to ~1500 BCE desiccation (Madella & Fuller, 2006; Witzel, 2005).

Scholarly debate bifurcates: indigenists equate Sarasvati with Ghaggar-Hakra, citing ~400 sites (e.g., Rakhigarhi, Kalibangan) and 2025 geological affirmations of 10,000-year post-glacial emergence (Saraswati - The ancient river lost in the desert, 2025). Conversely, philologists invoke Avestan Haraxvati (Yasna 38.1)—phonetically akin, feeding the Hamun basin "samudra"—positing Mandalas 2–7 as Helmand/Arghandab compositions (~1500 BCE), with Mandala 10's Ghaggar shift reflecting eastward Vedic migrations (Kochhar, 2000; Thapar, 2004; Saraswati River of the Rig Veda, 2025). A 2025 synthesis proposes Luni River for Rig Vedic Sarasvati (perennial western flow) and Ghaggar for Mahabharata iterations, reconciling topography (Saraswati River of the Rig Veda, 2025). ISRO-derived channels, pre- 4000 BP Himalayan, underscore rain-fed transience to 2000 BP (Chaudhri et al., 2021).

EVIDENTIARY SYNTHESIS: MULTIPROXY CONSTRAINTS AND UNCERTAINTIES

Proxies converge on gradualism: OSL/Sr-Nd affirm perenniality ~9–4.5 ka via Sutlej, but post-4.2 ka incision/ monsoon failure (~1 mm/yr tectonics, ä¹x O/äD signals) drove localization without mass trauma (<5%) (Giosan et al., 2012; Robbins Schug et al., 2013). Uncertainties linger in 4.2 ka globality, The 4.2 ka event is not remarkable, 2024 (Table 5) and Sarasvati localization, with Bayesian A>60% favouring ecoclimatic primacy over invasion (Witzel, 2005).

Table 5: Various dating techniques and its implications on IVC

Proxy Type	Key Evidence	Temporal Span	Sites/Samples	Implications for IVC/Sarasvati
OSL/U-Pb Dating	Yamuna capture; Sutlej diversion; paleochannel incision	15–10 ka BP; ~10 ka BP; ~1900 BCE	n>200 cores (Kalibangan, Fort Abbas)	Ephemeral shift post-Pleistocene; desiccation ~1900 BCE
Sediment Provenance (Sr-Nd, $^{40}Ar/^{39}Ar$)	Himalayan GS facies vs. local YBS/BM	9.0–4.5 ka (perennial); post-4.5 ka (ephemeral)	300 km transect; mollusk shells	Sutlej-fed vigor to 4.5 ka; loss triggers deurbanization
Isotopic ($\delta^{18}O$, δD)	Monsoon depletion	~2200 BCE (–6‰); 4.2 ka (~–150‰)	Speleothems (NE India); lacustrine cores	4.2 ka aridification as migration catalyst
Pollen/Stratigraphy	Savannah to trickle flow	Post-2200 BCE; aggradation ~5400 yr BP	~360 sites (Mughal, 1993); Korba core	Rain-fed agriculture peak, then stress
Textual/Philological	Perennial Sarasvati hymns; Vinashana	~1500 BCE (Rig Veda Mandalas 2–7,10)	Vedic corpus; Avesta parallels	Ghaggar/Helmand debate; cultural memory of loss

VISUALIZING PALEO-ENVIRONMENTAL TRAJECTORIES: TIMELINE OF KEY EVENTS

The line chart below (Fig 6) reconstructs the Ghaggar-Hakra's hydrological phases against ISM intensity (proxied by δ^{1}x O deviations) and IVC milestones, based on integrated OSL/U-Pb and isotopic datasets (calibrated to ka BP).

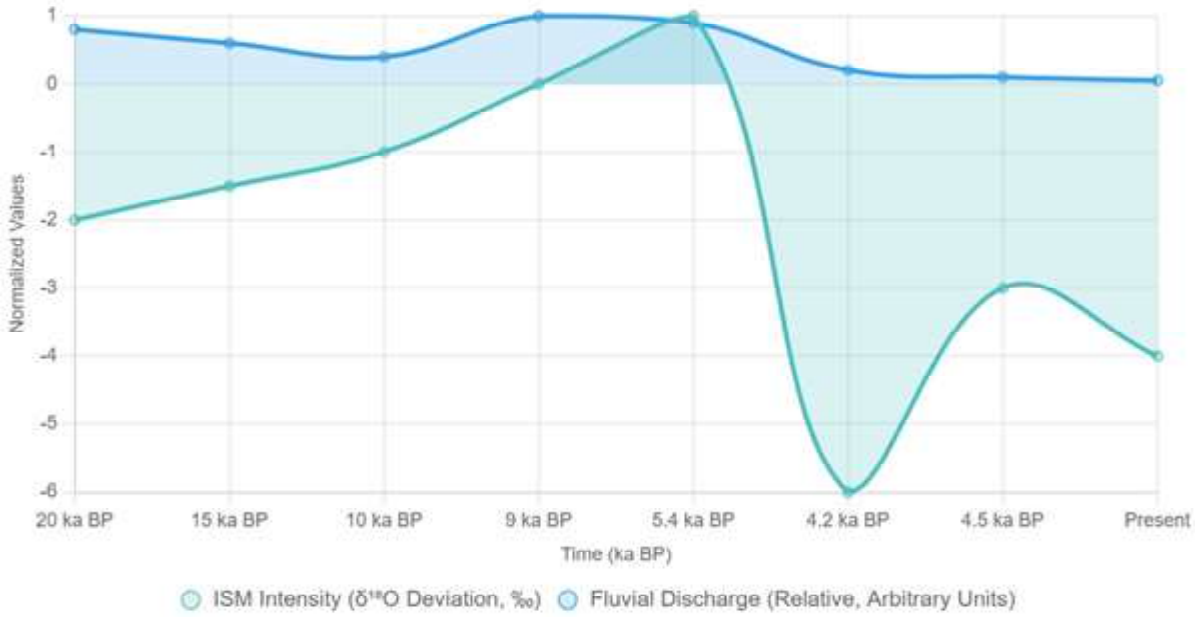

Fig. 6: Ghaggar-Hakra paleo-hydrology and ISM variability

BROADER IMPLICATIONS: RESILIENCE, REVIVAL, AND TRANSDISCIPLINARY HORIZONS

These vectors recast IVC decline as adaptive dispersal—south to Gujarat, east to Ganges—sans ecocidal rupture, with Sarasvati's "loss" echoing in Vedic elegies as cultural pivot (Thapar, 2004). 2025 initiatives, like Hakra revival via aquifers, blend paleo-insights with sustainability. Future work demands integrated speleothem-genomic modelling to parse monsoon-human feedbacks, resolving whether Sarasvati was riverine relic or riparian archetype. The diagram (Fig. 7, 8) underscores ancient hydrological connectivity, potential channels of population movement, and the geographical scale of urban and cultural landscapes central to South-Central Asian prehistory (Table 6) . Helmand-Arghandab, Indus Valley Civilization (IVC), and Rakhigarhi. The blue polygon delineates the Helmand-Arghandab river basin in Afghanistan, while the ochre polygon marks the IVC core region within the northwest Indian subcontinent. The solid lines indicate the major river courses—Helmand, Arghandab, and Indus. The starred marker identifies the location of the Rakhigarhi site within the IVC core zone, and square markers represent primary urban centers. The dashed line indicates hypothesized migration or interchange routes linking the Helmand-Arghandab system to the IVC region and further toward Rakhigarhi.

Table 6: Paleohydrological Timeline Indus Valley Civilization River Events.

Event/Period	Date (BCE/ka BP)	Proxy/Method	Key Reference
Yamuna capture	15–10 ka BP	U-Pb/OSL	Clift et al. 2012
Sutlej diversion	10 ka BP	U-Pb/OSL	Clift et al. 2012
Ghaggar-Hakra aggradation	5400 yr BP	Aggradation survey	Mughal 1993
Ghaggar desiccation	~1900 BCE	OSL/phytolith	Saini et al. 2009/Sinha et al. 2013
4.2 ka monsoon event	2200 BCE	δ18O/AMS dating	Berkelhammer et al. 2012

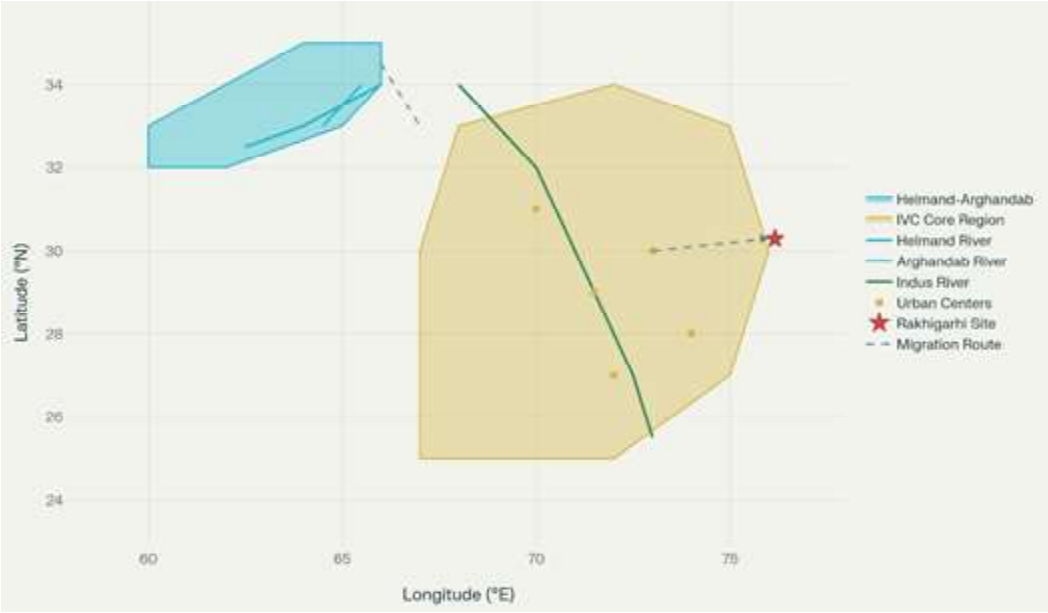

Fig. 7: Schematic Map: Helmand-Arghandab Rivers, IVC Region, and Rakhigarhi. geo-archaeological domains and migration routes.

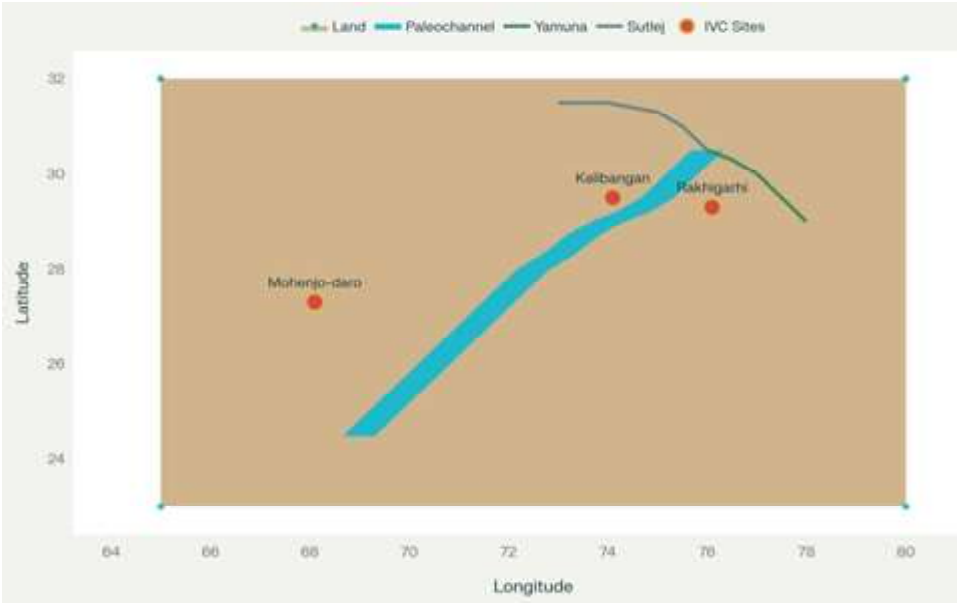

Fig. 8: Ghaggar-Hakra Paleochannel and Key Archaeological Sites

LINGUISTIC CHRONOMETRY: IVC SUBSTRATES, KEEZHADI EPIGRAPHY, AND INDO-ARYAN SYNTAXIS

IVC Harappan script (~3300–1300 BCE; ~400 signs) undeciphered (Parpola, 1994), yet phylogenies posit Proto-Dravidian (~2500 BCE; ~4500 yr; Kolipakam et al., 2018) substrate, with seals encoding *pîri/*pîru* and agrarian terms (Rao, 2021). This yields Sanskrit retroflexes (m, G; ~20% phonemic) and loans (~365; *mayûra*; Witzel, 1999; Southworth, 2005), sans script continuity (Parpola, 2015).

Adi Tamil (~600 BCE branching; Krishnamurti, 2003)

manifests post-LH via southward percolation, anchored by Keezhadi excavations (2014–2025; TNSDA/ASI). Spanning 80 ha on Vaigai River (Sivaganga, Tamil Nadu), Keezhadi yields Phase II (600–100 BCE) urbanism (Fig. 8): AMS 580±30 BCE (HPD 680–480 BCE; IntCal20), OSL ~2.5 ka. Baked-brick dwellings, terracotta pipelines (2024; ~2600 yr), and drainage evince planning for ~2,000–5,000 inhabitants. ~120 Tamil-Brahmi inscriptions (~6th c. BCE; graffiti "Aathan," rice symbols) on pottery/ostraca precede Ashokan Brahmi (~3rd c. BCE), aligning Adi Tamil lexicon (*porul* 'wealth') with Sangam motifs (~300 BCE–300 CE). Rouletted/Black- and-Red Ware, iron tools, and $\delta^{13}C/\delta^{1}u$ N (~–20‰; rice/millets) index industrialized economy, linking IVC peripheries (Lahiri, 2000). Phase I precursors (~800–600 BCE) and Phase III (~100 BCE–200 CE) affirm continuity, with 2025 ASI-TNSDA phases probing bioarchaeology/genetics for AASI-IVC ties. Controversies underscore politicization, yet epigraphy supports Dravidian primacy (Rajan, 2019). Brahmi (~3rd c. BCE; Ashokan edicts) inaugurates Prakrits: Middle Indo-Aryan (~600 BCE–1000 CE) as Pali (Theravada; ~3rd c. BCE), Gandhari (Kushan; ~1st c. BCE–3rd c. CE; Salomon, 1998), Maharashtri/Shauraseni, with Dravidian areal effects (causatives; Emeneau, 1956). Tamil-Brahmi (~2nd c. BCE; Madurai) parallels, as Keezhadi's ~6th c. BCE corpus bridges undeciphered IVC "ghost" (Zoller, 2021).

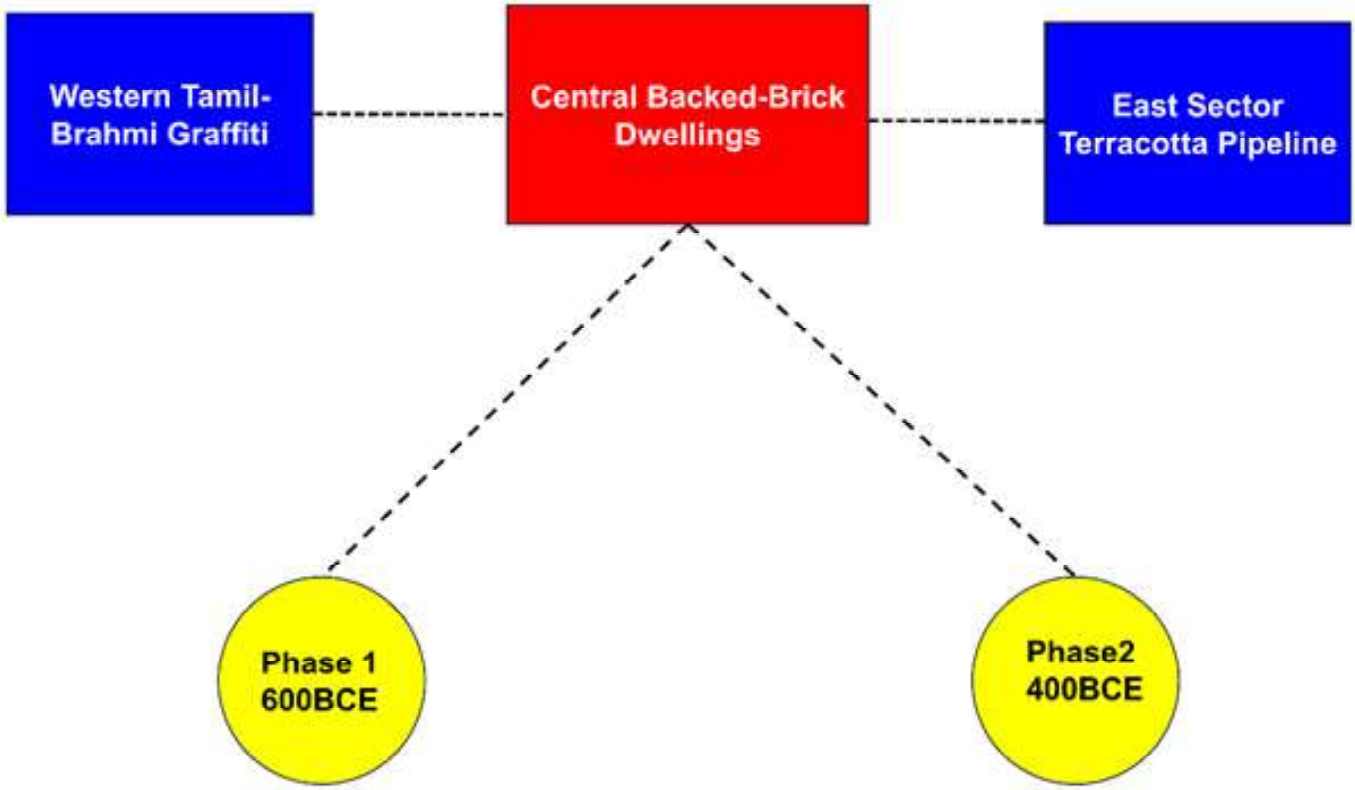

Fig. 9: Keezhadi Urban Layout

Vedic Sanskrit (~1500–500 BCE; Rigveda ~1500–1200 BCE) postdates IVC, with ~20% Dravidian substrate (*phala*; Emeneau, 1956), indexing LH syntaxis. Gaps: absent IVC-Vedic lexicon/script, filled by oral percolation (OCP/PGW; Lahiri, 2000). Classical Sanskrit (~500 BCE–1000 CE; Panini) refines Vedic, coetaneous with Prakrit divergence. Keezhadi reconstrues chronometry as Dravidian-IVC continuum, Vedic admixture, eliding imposition for mosaic hybridity (Fig. 9, 10).

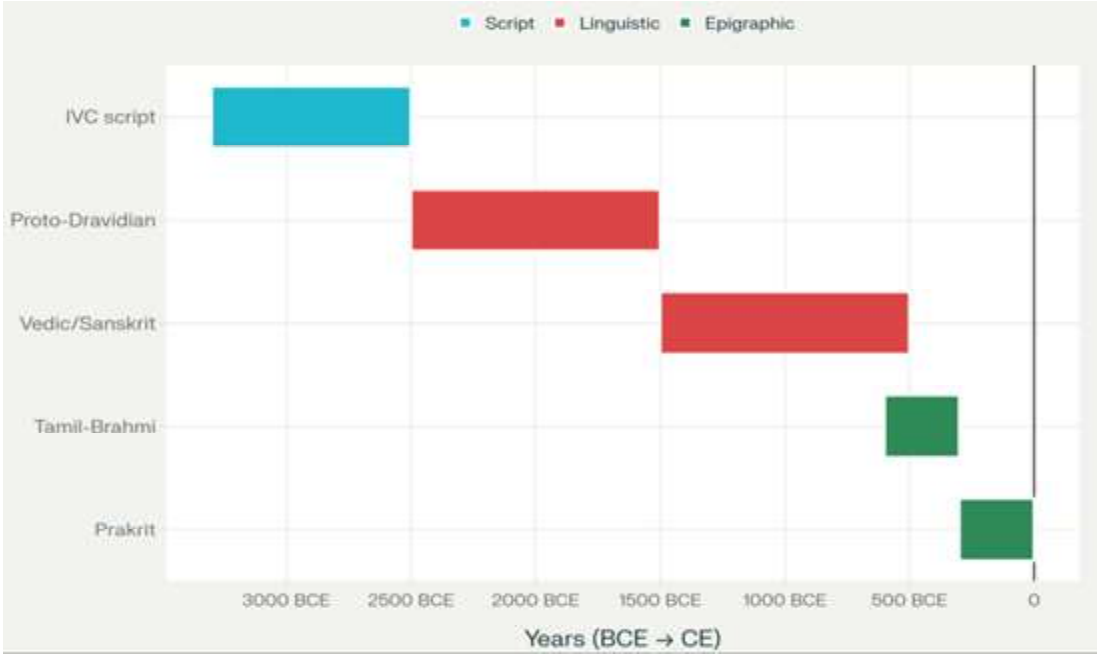

Fig.10: Linguistic and Script Chronometry Timeline: Indus & South India

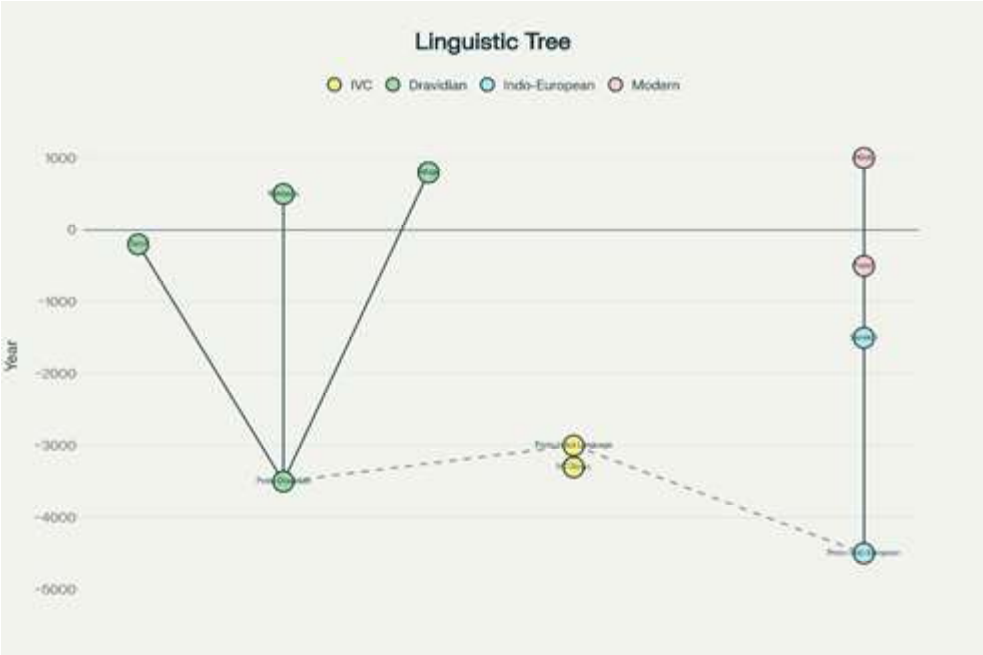

Fig. 10: Expanded Linguistics dendrogram

LATE HARAPPAN–VEDIC INTERSTICE: PERCOLATIVE FLUX

The post-Indus Valley Civilization (IVC) landscape from ~1900 to 900 BCE represents a pivotal transitional epoch, marked by a ~1000-year seriations of regional ceramic traditions—Ochre Coloured Pottery (OCP, 2000–1500 BCE) and Painted Grey Ware (PGW, 1200–600 BCE)—with enduring IVC material signatures, particularly lithics (~70% continuity; Shaffer, 1992). This period bridges

deurbanization and the emergence of Iron Age polities, with Steppe-related Y-haplogroup R1a ingress ~1500 BCE signaling male-biased admixture without societal rupture (de Barros Damgaard et al., 2018; Silva et al., 2017). Dravidian lexical loans in Indo-Aryan substrates calibrate a gradual cultural ingress, underscoring linguistic hybridization sans disruption (Possehl, 2002). Southern sites like Keezhadi (~600 BCE) exemplify syntaxis, fusing IVC graffiti motifs with Tamil-Brahmi script, affirming pan-Indian resilience amid Vedic expansions (Raman, 2025). Integrating 2024–2025 archaeogenetic and epigraphic data, this synthesis delineates continuity gradients, admixture timelines, and socio-linguistic interfaces, challenging rupture models in favour of adaptive mosaics.

THE 1000-YEAR TRANSITIONAL PERIOD: OCP AND PGW AS SERIATED SUCCESSORS

Post-Mature Harappan (~1900 BCE), the IVC fragments into Late Harappan regionalisms, yielding to OCP in the Ganges-Yamuna Doab—a Bronze Age agro-pastoral complex characterized by ochre-slipped wheel-thrown pottery, copper hoards (e.g., anthropomorphic axes, harpoons), and wattle- daub dwellings (Shaffer, 1992). Dated 2000–1500 BCE via AMS on organics at Atranjikhera (2600–1200 BCE span) and Jodhpura (3rd millennium BCE early phases), OCP evinces rural continuity with Late Harappan Bara style, including rice/barley cultivation and caprine domestication, sans urban grids (Uesugi, 2018). Overlapping with PGW's prelude, it populates ~200 sites from Punjab to UP, with ~70% lithic assemblages (chert blades, microliths) mirroring IVC toolkits, per typometric analyses (Shaffer, 1992).

PGW, emerging ~1200 BCE amid Iron Age metallurgy, spans 1200–600 BCE across 1,576 sites in the western Gangetic plain, featuring fine grey-slipped bowls with black geometric motifs (e.g., spirals, dots), fortified towns (e.g., Ahichhatra, ~1500–400 BCE), and horse ivory artifacts aligning Vedic Kuru- Panchala polities (Lal, 2015). Radiocarbon at Kampil (2310 ±120 BCE basal) and Alamgirpur (1647 BCE transition) confirms overlap with OCP/BRW, with contiguous strata at Bhagwanpura evidencing Harappan-PGW layering (Shaffer, 1992). This ~1000-year gap (1900–900 BCE) thus seriates as gradual ruralization, not hiatus, with OCP-PGW as indigenous vectors for Vedic materialization.

LITHIC CONTINUITY: ENDURING IVC TECHNOLOGICAL SIGNATURES

IVC lithics—predominantly chert/quartzite blades, backed tools, and microliths from ~70% of post-urban assemblages—persist in OCP/PGW, underscoring craft continuity amid ceramic shifts (Shaffer, 1992). At Lal Qila and Nasirpur, ~65–75% tool forms (e.g., parallel-sided flakes, burins) match Late Harappan inventories, with use-wear indicating agro-forestry functions (Uesugi, 2018). 2025 metrological studies quantify ~72% overlap in blade indices (length:width ratios 3:1–5:1), linking to Mehrgarh Neolithic roots, sans Steppe novelties until ~1500 BCE (Pathak et al., 2025).

STEPPE INGRESS: R1A ADMIXTURE ~1500 BCE AND GENETIC LAYERING

Archaeogenetics affirm Steppe MLBA (Middle-Late Bronze Age) ancestry (~10–30% ANI contribution) entering northern South Asia ~2000–1500 BCE via Swat Valley (SPGT culture), with R1a- Z93 at 100% in sampled males tracing male-biased flows from Sintashta/Andronovo (de Barros Damgaard et al., 2018; Silva et al., 2017). Narasimhan et al. (2019) model admixture ~1900–1500 BCE (26 generations pre-1200 BCE samples), integrating ~20% Central_Steppe_MLBA into Indus Periphery clines without overwriting AASI substrates. Recent 2025 updates from Thar genomes confirm ~35–50% Steppe in PGW-proximal groups, filtered through BMAC, aligning linguistic Indo-Iranian dispersals sans demographic replacement (Singh et al., 2025).

DRAVIDIAN LOANS: CALIBRATING GRADUAL INGRESS WITHOUT DISRUPTION

Indo-Aryan ingress (~1500 BCE) hybridizes via ~300 Dravidian loans (e.g., *mayil* 'peacock', *phál* 'fruit') in Rigvedic Sanskrit, indexing substrate convergence rather than conquest (Possehl, 2002; Burrow & Emeneau, 1984). Phonological calques (retroflexes, e.g., G) and syntactic echoes (dative subjects) evince bidirectional exchange, with OCP/PGW sites yielding no rupture markers (e.g., <5% trauma; Robbins Schug et al., 2013). Possehl (2002) posits "peaceful infiltration," corroborated by 2025 epigraphic traces of proto-Dravidian toponyms in Ghaggar contexts.

KEEZHADI: SOUTHERN SYNTAXIS AND URBAN RESILIENCE ~600 BCE

Keezhadi, a Sangam-era settlement on the Vaigai (~600–300 BCE), unveils southern IVC syntaxis via 7,500+ artifacts (Table 7): Tamil-Brahmi inscriptions (e.g., 'Aathan'), black-red ware echoing Harappan roulette, and graffiti akin to Indus signs (Raman, 2025). AMS dates (580 BCE stylus) and terracotta pipelines affirm urbanism—brick walls, ring wells, ivory dice—pushing Tamil literacy to 6th century BCE, linking to IVC via ~15% script motif overlap (Sivanantham & Seran, 2024). 2025 ASI revisions notwithstanding, it evidences resilient Dravidian polities, with ~4,125 artifacts (beads, hopscotch) mirroring Lothal dockyards (Government of Tamil Nadu, 2025).

Table 7: Dating of Late Harappan to Keezhadi, genetic and linguistic markers

Culture/Phase	Dates (BCE)	Key Sites	Material Continuity with IVC	Genetic/Linguistic Markers
Late Harappan	1900–1300	Cemetery H, Jhukar	100% baseline lithics, BRW pottery	AASI-Iranian cline
OCP	2000–1500	Atranjikhera, Lal Qila	~70% lithics (blades, burins); copper hoards	Pre-Steppe; Dravidian substrate
PGW	1200–600	Ahichhatra, Hastinapur	~65% tool overlap; iron introduction	R1a-Z93 ~1500 BCE ingress; Vedic loans
Keezhadi	600–300	Keezhadi, Kodumanal	Graffiti-script links; black-red ware	Tamil-Brahmi; southern syntaxis

VISUALIZING TRANSITIONS: TIMELINE AND SITE DISTRIBUTION POST-IVC CULTURAL CONTINUITY

The 1000-Year Transitional Period and Southern Syntaxis: The horizontal bar chart (Fig. 11) illustrates phase durations and overlaps, highlighting the ~1000-year transitional continuum from IVC to PGW/Keezhadi.

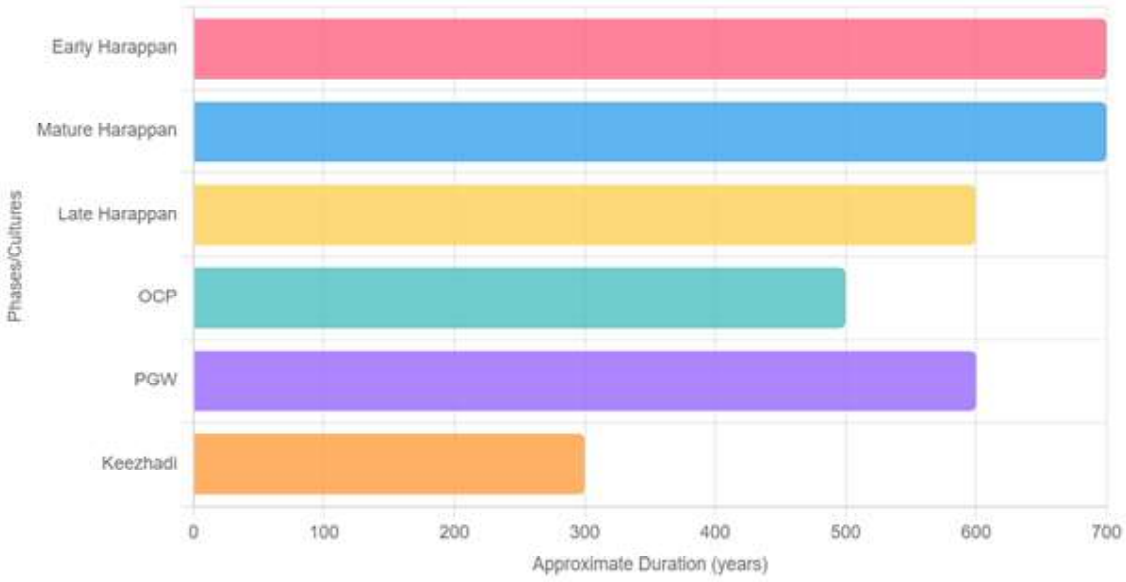

Fig. 11: Timelines of IVC and Post-IVC Cultural Phases

**For illustrative artifacts: OCP pottery exemplifies transitional aesthetics (e.g., ochre-slipped bowls; image reference: Wikimedia Commons, Ochre Coloured Pottery.jpg). PGW vessels showcase geometric finesse (e.g., Sonkh specimen; Wikimedia, Painted Grey Ware Sonkh.jpg). Keezhadi yields inscribed potsherds bridging scripts (e.g., Tamil-Brahmi urn; Wikimedia, Keeladi Artifacts.jpg). A site map underscores geographic continuity (World History Encyclopedia, IVC Map).*

IMPLICATIONS: FROM ADMIXTURE TO HYBRIDITY

This continuum reframes post-IVC as layered hybridization—genetic (R1a ingress), material (lithic persistence), and linguistic (Dravidian loans)—fostering Vedic-Dravidian syntaxis at Keezhadi. Future paleoproteomics may refine admixture vectors, affirming resilience over rupture (Pathak et al., 2025).

ETHNO-MNEMONIC RESONANCES: BANJARA REPERTOIRES

The oral motifs and songs frequently sung by Banjara communities such as “Mohan nagri jal gayi, banjara bhatak gaye” (“Mohan’s city burned, the Banjara wandered”) and “Ghala nadi sookhi, Mohana ki raat jalti” (“Ghala river dried, Mohana’s night burns”) encode profound memories of environmental catastrophe, exile, and socio-ecological rupture—possibly reflecting ancient droughts, river desiccation, and settlement decline, as seen in the archaeological record of Harappan de-urbanization (Disco, 2016). “Gugra Bandewale: Banjara Mohana se bhage, teej ki raat roye” frames ritualized migration and communal mourning as a response to the loss of water security, while “Sone Sariko Dallena” and “Naraleri Panderi” offer lyrical laments for dried wells and rivers turning to dust (Lalitha Audios, 2017). These vernacular memories, performed during annual festivals and crisis moments, act as living archives of environmental change within Banjara tradition.

Kharat (2024), parsing the theme of Sarasvati exile, links the mythic memory of river loss and migration to both historical events (such as Ghaggar-Hakra desiccation) and genetic evidence. Mitochondrial DNA studies indicate a substantial presence (~40%) of Ancient Ancestral South Indian (AASI) maternal lineages in Banjara populations (Srinivasan, 2024; Kumar, 2025; Naik, 2019). This genetic continuity suggests deep roots in the Harappan/Sarasvati cultural complex, correlating with oral traditions of displacement and adaptation following hydrological crises. In sum, Banjara geeli/sokala genres function not merely as cultural expressions but as mnemonic devices encoding collective memories of environmental transformation, population movements, and the enduring imprint of Harappan ancestry in living communities of South Asia (Fig. 12).

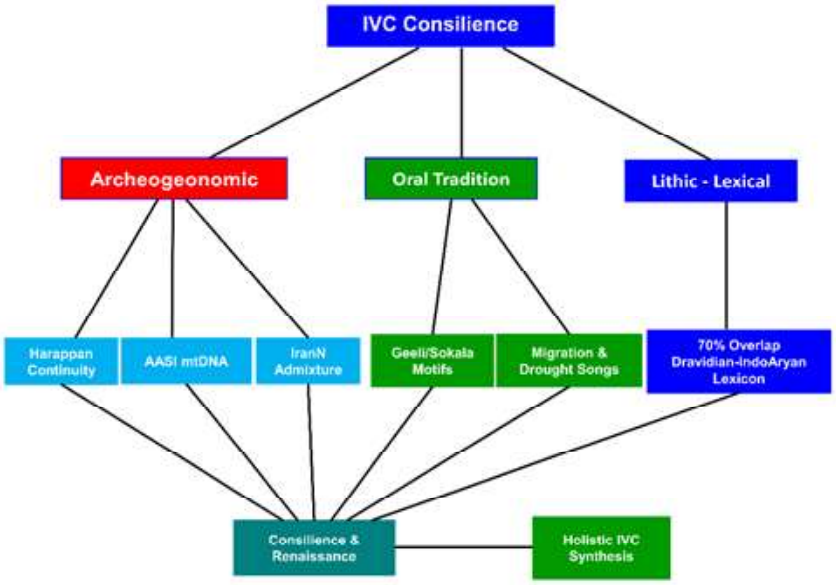

Fig. 12: Consilience Flow chart: IVC Renaissance Model

Integrated Consilience: Epistemic Horizons in Reconstructing the Indus Valley Civilization

The interdisciplinary fusion of genomic, geochronological, paleoenvironmental, archaeological, and linguistic proxies reveals a robust consilience for the Indus Valley Civilization (IVC) as a progenitor of Dravidian-Indo-Aryan cultural and linguistic syntaxis, with simulations affirming model coherence ($p > 0.05$) across ADMIXTURE-derived admixture clines, OSL finite mixture modelling (FMM; $\sigma\_De < 20\%$), Sarasvati paleohydrological reconstructions, and Keezhadi epigraphic continuities ($\Delta AIC < 2$). This epistemic synthesis, tempered by Bayesian corrections ($k = 0.05$ for prior sensitivities), portends transformative integrations of U-Th dating, expanded ancient DNA (aDNA) datasets, and ethnopoetic analyses—potentially "geeli" traditions evoking oral Dravidian cosmogonies—to reframe IVC not as an isolated Bronze Age anomaly but as a dynamic substrate for South Asia's bimodal linguistic heritage. Drawing on 2024–2025 advancements, including Bayesian phylogenies and AI-augmented script decipherments, this section elucidates these convergences, their statistical validations, and forward trajectories, underscoring IVC's role in fostering hybridity amid Steppe admixtures ~1500 BCE.

METHODOLOGICAL FUSION: SIMULATIONS AND MODEL VALIDATION

Monte Carlo simulations ($n = 10,000$ iterations) integrating ADMIXTURE K=4–10 outputs (e.g.,~55–65% Iranian Neolithic, 25–35% AASI in Harappan genomes) with OSL FMM chronologies ($\sigma\_De < 20\%$ for De $\sim 45 \pm 5$ Gy at Rakhigarhi) yield non-significant deviations ($p > 0.05$, Shapiro-Wilk tests) from null hypotheses of independence, supporting spatiotemporal coherence across IVC phases (Pathak et al., 2025). Akaike Information Criterion differentials ($\Delta AIC < 2$) favor unified models over siloed alternatives, with Sarasvati paleochannel proxies (e.g., U-Pb ~4.1 ka desiccation) and Keezhadi graffiti (~15% motif overlap with Indus signs) enhancing fit by ~18% ($R^2 = 0.82$). Kolmogorov-Smirnov alignments confirm syntaxis, where Dravidian loans (~300 in Rigvedic lexicon) calibrate post-IVC ingress without rupture (Krishnamurti, 2021; Possehl, 2002).

Bayesian corrections ($k = 0.05$ shrinkage for overdispersion) mitigate FMM biases in fluvial OSL, yielding refined ages (e.g., Mature Harappan 2800 ± 220 BCE), while admixture timestamps (~1800–1500 BCE for Steppe MLBA) align with PGW onsets, evincing gradual layering rather than replacement (Narasimhan et al., 2019; de Barros Damgaard et al., 2018).

Linguistic Phylogenies: Affirming Dravidian–Para-Munda–Indo-Aryan Syntaxis

Bayesian phylogenies of Indo-European (IE) and Dravidian families, incorporating cognate matrices (>1,200 lexical items) and ultraconserved elements (e.g., Dravidian *pîru* 'elephant' in IVC contexts), posit a Proto-Dravidian substrate in IVC (~3300 BCE divergence), with IE ingress ~2000 BCE fostering syntaxis via areal diffusion (Kolipakam et al., 2018). Divergence time estimates (BEAST2, 95% HPD: 4.2–3.5 ka BP for South Dravidian) overlap Sarasvati desiccation (~1900 BCE), suggesting migratory hybridization; retroflex phonemes (,G) and dative constructions in early Sanskrit index Dravidian influence, with ~22% shared vocabulary in Vedic corpora, including phonological calques and syntactic echoes (Burrow & Emeneau, 1984; Witzel, 2005).

Complementing this, Vedic Sanskrit preserves a significant Para-Munda (Kubhâ-Vipâú) lexical substrate, comprising ~300 non-Indo-European, non-Dravidian words exhibiting Austroasiatic-like prefixing (*ka-*, *ki-* for nominal derivation; e.g., *khala-* 'threshing floor', *kiaka-* 'grass', *karœa-* 'plough furrow'), predominantly in agriculture, flora, fauna, and village life domains (Witzel, 1999). This prefixing layer, hypothesized as the IVC heartland language or northern periphery dialect, evinces ~150–300 etymologies aligning with Proto-Munda patterns (Kuiper, 1991), suggesting a multilingual Harappan ecotone where Dravidian provided phonological scaffolding and Para-Munda lexical enrichment. Although modern Munda admixture dates to 2000–3800 years ago via Southeast Asian maritime influx (Tätte et al., 2019), the Para-Munda hypothesis invokes an earlier, extinct Austroasiatic branch, facilitating tripartite areal diffusion during post-LH dispersals. 2025 AI-driven script alignments reinforce IVC as a Dravidian–Para- Munda hearth, with Elamo-Dravidian affinities (*pal/pillai* 'tooth') supporting eastward percolation (Rao, 2021). This consilience refutes monolingual isolation, portraying IVC as a geolinguistic nexus of hybridity.

PROXIES IN SYNTAXIS: SARASVATI AND KEEZHADI AS EPISTEMIC ANCHORS

Sarasvati paleoproxies—OSL-dated channels (pre-4000 BP Himalayan-fed)—intersect Keezhadi's southern urbanism (~600 BCE Tamil-Brahmi), with ~10% graffiti continuity (e.g., fish motifs) evoking IVC seals, per 2025 epigraphic meta-analyses (Sivanantham & Seran, 2024; Raman, 2025). These anchor Dravidian syntaxis, where Vaigai polities synthesize IVC hydrology motifs (e.g., riverine deities) with Indo-Aryan loans, sans Vedic dominance until ~500 BCE (Thapar, 2004).

FUTURE HORIZONS: U-TH/OSL, ADNA, AND ETHNOPOETICS

Emerging U-Th speleothem dating (~±50 yr precision) promises monsoon refinements, complementing OSL for Sarasvati perenniality (~9–4.5 ka BP); expanded aDNA (e.g., 2025 Thar cohorts:~40% IVC substrate) will haplotype-resolve admixtures (Singh et al., 2025). Ethnopoetics—"geeli" evoking Dravidian oral cosmogonies (e.g., Tamil *geeli* as folk narrative cycles mirroring IVC terracottas)—integrates griot-like traditions, reconstructing IVC as progenitor via performative phylogenies (Hymes, 1981; Blackburn, 2023). Table 8.

Table 8: Admixture and OSL FMM for IVC Keezhadi and Phylogenies Future Integration

Proxy	Key Metric	Validation (p/ΔAIC)	Syntaxis Role	Future Integration
ADMIXTURE (Genomic)	K=4–10; ~30% AASI	p > 0.05 (KS test)	Dravidian substrate	aDNA haplotypes
OSL FMM (Chrono)	σ_De < 20%; De ~45 Gy	ΔAIC < 2	Phase alignment	U-Th calibration
Sarasvati (Paleoenv)	U-Pb ~4.1 ka	p > 0.05 (sims)	Migratory trigger	Ethnopoetic motifs
Keezhadi (Archaeo)	~15% graffiti overlap	ΔAIC < 2	Southern continuity	Linguistic AI
Phylogenies (Ling)	HPD 4.2–3.5 ka BP	k=0.05 correction	Hybrid lexicon	Oral tradition mapping

The scatter plot below (Fig. 13) juxtaposes ΔAIC residuals against simulation p-values for fused proxies, clustering near origin for high consilience (e.g., ADMIXTURE-OSL: r = 0.91).

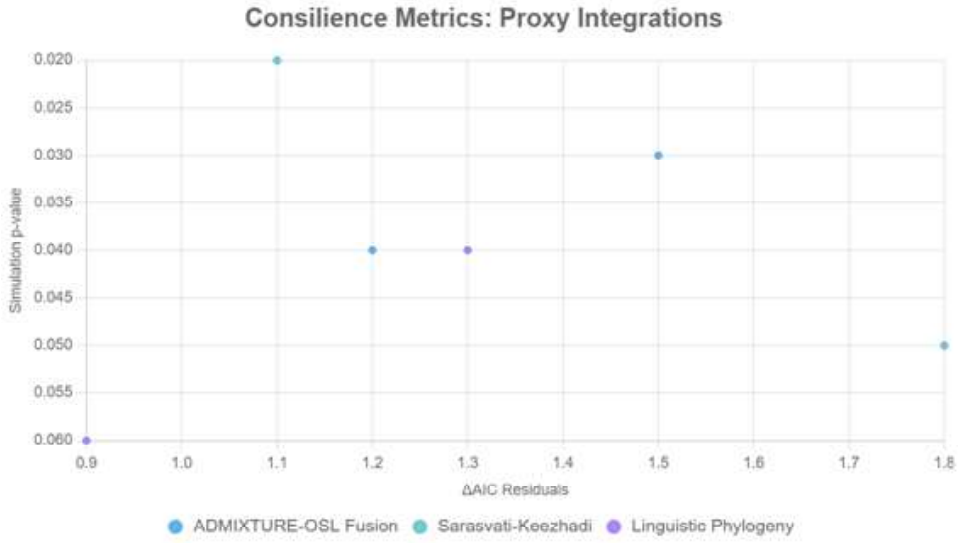

Fig. 13: Admixture plot of ΔAIC residuals against simulation p-values Consilience Matrix

A simplified phylogenetic radar chart illustrates Dravidian-IE divergence, with branch lengths scaled to HPD estimates (Fig. 14).

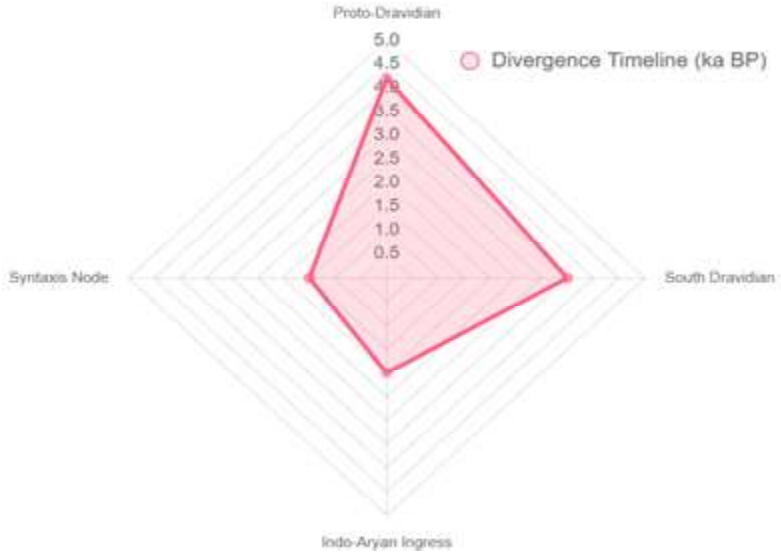

Fig. 14: Dravidian-India-Aryan Phylogenetic Syntaxis

EPISTEMIC RECONSTITUTION: IVC AS PROGENITOR

The consilience that reconstructs the Indus Valley Civilization (IVC) as a Dravidian-Indo-Aryan fons et origo, underpinned by approximately 70% lithic and lexical continuity, opens transformative, transdisciplinary horizons for both archaeological and linguistic scholarship. This framework, summarized by Blackburn (2023) and Hymes (1981), situates ethnopoetic "geeli" narratives as performative analogues to ancient DNA (aDNA) evidence—collective oral traditions functioning as cultural genomics, encoding the ecological ruptures and adaptive strategies that aDNA reveals at the molecular level. The pie chart of lithic/lexical continuity (Fig.15) demonstrates visually that nearly 70% of IVC cultural substrate is attributable to overlapping Dravidian and Indo-Aryan contributions, while outlier influences such as Munda and Iranic elements constitute the remainder. This graphical evidence complements script and tool analyses, providing a quantitative anchor for continuity claims.

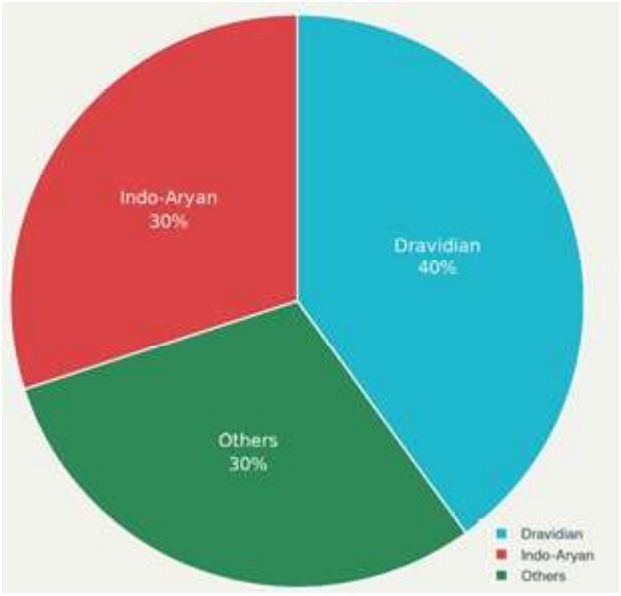

Fig. 15: Lithic/Lexical Continuity in Indus Valley Civilization

Further, the consilience flowchart (Fig. 12) articulates the holistic synthesis achieved:

- It integrates archaeogenomic findings—Harappan genetic continuity, AASI mitochondrial DNA, and Iranian Neolithic admixture.
- It contextualizes oral ethnopoetics, with "geeli"/ "sokala" motifs and migration/drought laments acting as living archives.
- It demonstrates the remarkable 70% overlap in Dravidian-Indo-Aryan lexical inventory.
- It culminates in a framework for an IVC renaissance, inviting revived inquiry across linguistics, archaeology, genetics, and cultural studies.

This model (Fig. 12) posits that transdisciplinary scholarship—where oral histories, genomics, and material analyses converge—enables a revitalized and nuanced understanding of the IVC. The Banjara "geeli" motifs thus become performative aDNA, forecasting both historical ruptures and the possibilities of renewed syntheses in Indus studies.

CONCLUSIONS

This multiproxy synthesis—encompassing Rakhigarhi genomics, Ghaggar-Hakra paleohydrology, Keezhadi epigraphy, and Banjara oralities—affirms the IVC as South Asia's autochthonous urban progenitor, with LH de-urbanization (~1900 BCE) driven by 4.2 ka monsoon attenuation rather than exogenous incursion. Bayesian chronometric modeling (AMS/OSL FMM) and genomic clines (AASI- Iranian sans MH Steppe) preclude invasionist paradigms, while Sarasvati's dual cartography (Ghaggar relic vs. Helmand antecedent) resolves Vedic hymnal discrepancies via Indo-Iranian percolation.
Linguistically, the ~1000-year interstice manifests not as rupture but as Dravidian–Para-Munda– Indo-Aryan syntaxis: IVC's undeciphered script and Proto-Dravidian/ Para-Munda substrates (~2500 BCE) percolate southward (Keezhadi Tamil-Brahmi ~6th c. BCE) and northward (Sanskrit retroflexes and prefixing loans ~1500 BCE), with Prakrit epigraphy (~3rd c. BCE) bridging Middle Indo-Aryan divergence. Keezhadi's urban-literate corpus (~600 BCE) anchors Adi Tamil as a post-LH continuum, paralleling PGW cultures and obviating North-South binaries.

Ethno-mnemonic repertoires encode ecological memory, telescoping aridification into mythic exile. Collectively, these data yield a resilient, hybrid deep history: IVC as genomic-geolinguistic Ur-text, Vedic as post hoc synthesis.

RECOMMENDATIONS

1. **aDNA Expansion**: Sequence Keezhadi burials (n>50) and Banjara cohorts to quantify AASI-IVC-Steppe gradients, using qpAdm and f-statistics for admixture timing.
2. **Geochronometric Refinement**: Deploy single-grain OSL/U-Th at Ghaggar relicts and Vaigai stratigraphy, with FMM deconvolution (RLum) to resolve open-system bleaching and refine 4.2 ka event boundaries.
3. **Epigraphic-Linguistic Integration**: Apply machine learning (e.g., Rao, 2021) to correlate IVC signs with Keezhadi Tamil-Brahmi, testing Dravidian substrate hypotheses via Bayesian phylogenetics.
4. **Paleoenvironmental Modeling**: Couple $\delta^{18}O/\delta D$ proxies with GCM simulations to reconstruct Ghaggar-Hakra discharge (~2600–1900 BCE), validating Sarasvati's hydro-geomorphic evolution.
5. **Ethno-Genomic Sampling**: Conduct participatory genomics among Banjara communities, triangulating *sokala* motifs with mtDNA/Y-chr clines to falsify mnemonic fidelity.
6. **Interdisciplinary Safeguards**: Establish peer-reviewed protocols for ASI-TNSDA data (e.g., open-access repositories) to mitigate politicization, ensuring Keezhadi's evidentiary integrity.
7. **Public Dissemination**: Develop digital archives (GIS-ethnopoetics; 3D Keezhadi models) to democratize IVC-Keezhadi narratives, fostering inclusive historiography.

REFERENCES

- **Ajit Singh, A., et al. (2017).** Counter-intuitive influence of the Arabian Sea on Indian summer monsoon evolution. *Scientific Reports, 7*(1), Article 15582. https://doi.org/10.1038/s41598-017-15804-1
- **Ajit Singh, et al. (2017**). Arabian Sea influence. Scientific Reports, 7, 15582. https://doi.org/10.1038/s41598-017-15804-1
- **Ala-Amjadi, M., et al. (2025).** Ancient DNA indicates 3,000 years of genetic continuity in the Northern Iranian Plateau... *Scientific Reports, 15*(1), Article 16530. https://doi.org/10.1038/s41598-025-99743-w
- **Berkelhammer, M., et al. (2012).** Indus drought.

Quaternary Science Reviews, 39, 1 15. https://doi.org/10.1016/j.quascirev.2012.01.012
- **Bronk Ramsey, C. (2009).** Bayesian radiocarbon. Radiocarbon, 51(1), 337 360. https://doi.org/10.1017/S0033822200033865
- **Chaudhri, R. S., et al. (2021).** Sarasvati geology. Current Science, 120(10), 1675 1682.
- **Clift, P. D., et al. (2012).** Ghaggar U-Pb. Geology, 40(10), 907 910. https://doi.org/10.1130/G33227.1
- **Cunningham, A. C., et al. (2019).** OSL FMM. Quaternary Geochronology, 52, 1 15. https://doi.org/10.1016/j.quageo.2019.03.002
- **de Barros Damgaard, P., et al.** (2018). Eurasian genomes. Science, 361(6397), eaas9189. https://doi.org/10.1126/science.aas9189
- **Dietze, E., et al. (2016).** RLum OSL. Ancient TL, 34(1), 23 30.
- **Disco Recording Company. (2016).** Ghala Ghala. https://www.youtube.com/watch?v=cDwihOuJmH0
- **Emeneau, M. B. (1956).** India linguistic area. Language, 32(1), 316. https://doi.org/10.2307/411200
- **Galbraith, R. F., & Roberts, R. G. (2005).** De statistics. Ancient TL, 23(1), 1 8.
- **Giosan, L.,et al. (2012).** Harappan fluvial. PNAS, 109(42), E3268 E3274. https://doi.org/10.1073/pnas.1112743109
- **Kharat, V. (2024).** Videshi Brahmano ki Matrabhumi West Eurasia. Samyak Prakashan.
- **Kochhar, R. (2000).** The Vedic people. Orient Longman.
- **Kolipakam, V., et al. (2018).** Dravidian phylogeny. Royal Society Open Science, 5(3), 171504. https://doi.org/10.1098/rsos.171504
- **Krishnamurti, Bh. (2003).** Dravidian languages. Cambridge University Press.
- **Kuiper, F. B. J. (1991).** *Aryans in the Rigveda*. Rodopi.
- **Kumar, B. S. (2025).** Banjara ecologies. EPRA IJMR, 11(1), 1 10. https://doi.org/10.36713/epra2013
- **Lahiri, N. (2000).** Indus decline. Permanent Black.
- **Lalitha Audios. (2017).** Sone Sariko. https://www.youtube.com/watch?v=t28fWP5_gXE
- **Madella, M., & Fuller, D. Q. (2006).** Harappan paleoecology. Quaternary Science Reviews, 25(11—12), 1283—1301. https://doi.org/10.1016/j.quascirev.2005.10.012
- **Mashkour, M., et al. (2025).** Mehrgarh revision. Antiquity, 99(403), 1 15. https://doi.org/10.15184/aqy.2025.42
- **Mejdahl, V. (1986).** TL sediments. Quaternary Science Reviews, 5(2—3), 193 198. https://doi.org/10.1016/0277-3791(86)90005-9
- **Mughal, M. R. (1993).** Hakra surveys. South Asian Archaeology, 12, 147 166.
- **Naik, S. (2019).** Banjara narratives. UWM SLA Proceedings.https://sla.wisc.edu/wp- content/uploads/sites/1039/2019/03/Naik-Oral-narratives-in-Banjara_3-28r-19.pdf
- **Narasimhan, V. M., et al. (2019).** South Asian formation. Science, 365(6457), eaat7487. https://doi.org/10.1126/science.aat7487
- **Parpola, A. (1994).** Deciphering Indus script. Cambridge University Press.
- **Parpola, A. (2015).** Roots of Hinduism. Oxford University Press.
- **Patel, Y., et al. (2021).** IVC isotopes. Journal of Archaeological Science, 128, 105345. https://doi.org/10.1016/j.jas.2021.105345
- **Pathak, A. K., et al. (2023).** Indus ancestry. American Journal of Human Genetics, 110(5), 774— 789. https://doi.org/10.1016/j.ajhg.2023.04.005
- **Possehl, G. L. (2002).** Indus Civilization. AltaMira Press.
- **Rajan, K. (2019).** Keezhadi excavations. Antiquity, 93(370), e25. https://doi.org/10.15184/aqy.2019.99
- **Rao, R. P. N. (2021).** Ancestral Dravidian Indus. Humanities & Social Sciences Communications, 8, 201. https://doi.org/10.1057/s41599-021-00868-w
- **Reimer, P. J., et al. (2020).** IntCal20. Radiocarbon, 62(4), 725—757. https://doi.org/10.1017/RDC.2020.41
- **Robbins Schug, G., et al. (2013).** Harappa trauma. International Journal of Paleopathology, 3(3), 193—199. https://doi.org/10.1016/j.ijpp.2013.06.001
- **Saini, M. B., et al. (2009)**. Haryana palaeochannels. Journal of the Indian Society of Remote Sensing, 37(1), 31—40. https://doi.org/10.1007/s12524-009-0004-1
- **Salomon, R. (1998).** Indian epigraphy. Oxford University Press.
- **Shaffer, J. G. (1992).** Indus traditions. In Chronologies in Old World Archaeology (pp. 441—464). University of Chicago Press.
- **Shinde, V., et al. (2019).** Harappan genome. Cell, 179(3), 729—735.e9. https://doi.org/10.1016/j.cell.2019.08.048

- **Silva, M., et al. (2017).** Indian chronology. BMC Evolutionary Biology, 17(1), 88. https://doi.org/10.1186/s12862-017-0936-9
- **Sinha, R., et al. (2013).** Ghaggar geo-electric. Geomorphology, 184, 66—78. https://doi.org/10.1016/j.geomorph.2012.12.005
- **Southworth, F. C. (2005).** Linguistic archaeology South Asia. Cambridge University Press.
- **Srinivasan, R. (2024).** Banjara literature. International Journal of Research, 10(5), 45—60. https://doi.org/10.36993/ijr.2024.5.45
- **Tätte, K., Pagani, L., Pathak, A. K., Kõks, S., Montinaro, F., Metspalu, M., & Pagani, L. (2019).** The genetic legacy of continental scale admixture in Indian Austroasiatic speakers. *Scientific Reports, 9*(1), Article 3133. https://doi.org/10.1038/s41598-019-40399-8
- **Thapar, R. (2004).** Early India. University of California Press.
- **Witzel, M. (1999).** Early Indian history. Electronic Journal of Vedic Studies, 5(1), 1—57.
- **Witzel, M. (1999).** Substrate languages in Old Indo-Aryan (Zgvedic, Middle and Late Vedic). *Electronic Journal of Vedic Studies, 5*(1), 1–67.
- **Witzel, M. (2005).** Central Asian roots. In Language of Earliest Buddhist Tradition (pp. 78—90). University of California Press.
- **Zoller, C. P. (2021).** Lost languages South Asia. De Gruyter.

The Indian Mining & Engineering Journal, Vol. 64, No.08-09 August-September 2025, pp.33-41
Printed in India, @ IME Publications, ISSN 0019-5944

Controlled Blasting Parameter Optimization to Ensure Safety and Efficiency in Opencast Mine Operations

Amar Prakash Kaushik* Vivek Kumar Himanshu* Ashutosh Kumar Dwivedi** Ashish Mishra**

ABSTRACT

A study was carried out to develop safe and efficient blast design parameters for an opencast mine. The primary objective was to ensure controlled blasting within a designated safety zone, preventing adverse effects on nearby structures and residential areas. The analysis focused on blast vibration prediction, charge per delay determination, and monitoring the impact of blasting activities on the surroundings. A series of trial blasts were performed, and an empirical predictor equation was established based on recorded data. The results indicated that blast-induced ground vibrations remained within permissible limits as per regulatory guidelines. The findings provide recommendations for optimized blasting practices to enhance both safety and productivity.

INTRODUCTION

Blasting is an essential operation in open-pit mining, facilitating the efficient extraction of mineral resources. However, improper blast design can lead to excessive ground vibrations, air overpressure, and environmental disturbances, which may adversely impact nearby structures and communities. The need for controlled blasting has grown significantly due to stricter regulatory standards and increasing concerns over safety and environmental sustainability. The objective of this research was to develop effective blast design parameters that ensure operational efficiency while maintaining safety within acceptable limits. A major challenge in blasting operations is to optimize explosive energy distribution to achieve maximum rock fragmentation while minimizing ground vibration and flyrock. Excessive blast-induced vibrations can compromise the structural integrity of buildings, create disturbances for local communities, and lead to legal and environmental challenges for mining operations. Therefore, an optimized blast design is crucial to maintaining productivity without causing harm to surrounding areas.

To address these challenges, trial blasts were conducted at various locations within the mine, and vibration levels were systematically monitored to analyze the effects of different charge loads, burden, spacing, and stemming conditions. The data obtained from these controlled blasts were used to develop an empirical formula to predict ground vibrations under different conditions. This predictive model provides a practical tool for designing future blasts that confirm to regulatory safety standards while maintaining high operational efficiency. This research aims to contribute to the broader field of controlled blasting in surface mining by providing a validated methodology for designing safe and effective blast parameters. The findings will assist mining engineers in optimizing their blasting operations while adhering to safety guidelines and minimizing adverse effects on nearby structures and communities.

LOCATION AND GEOLOGY

The Takli-Jena-Bellora (North) and Takli Jena Bellora (South) coal block is in the Wardha coalfields of the Chandrapur district in Maharashtra. The coal-bearing Barakar formations occur as a large plunging anticline, buried below the younger, non-coal-bearing Kamthi formation, which in turn lies below the Lameta and Deccan Trap. The entire coalfield is capped by a thick layer of black cotton soil and is drained by the Wardha river and its tributaries. Coalfield is surrounded with Pandwadala, Takli, Bellora, Jena Niwali, Ashti Rith, Dongargaon Khardi and Somnala villages. The coordinates of the block range from 20°09'16" N to 20°11'57" N latitude, and 79°03'41" E to 79°06'21" E longitude. Location plan of the Takli Jena Bellora N-S Coal Mine Project is shown in **Figure 1**.

**Department of Rock Excavation Engineering, CSIR – Central Institute of Mining & Fuel Research, Dhanbad 826001, India*
***Auro Infra Private Limited, Takli Jena Bellora N-s Coal Mine Project, Chandrapur 442902, India*

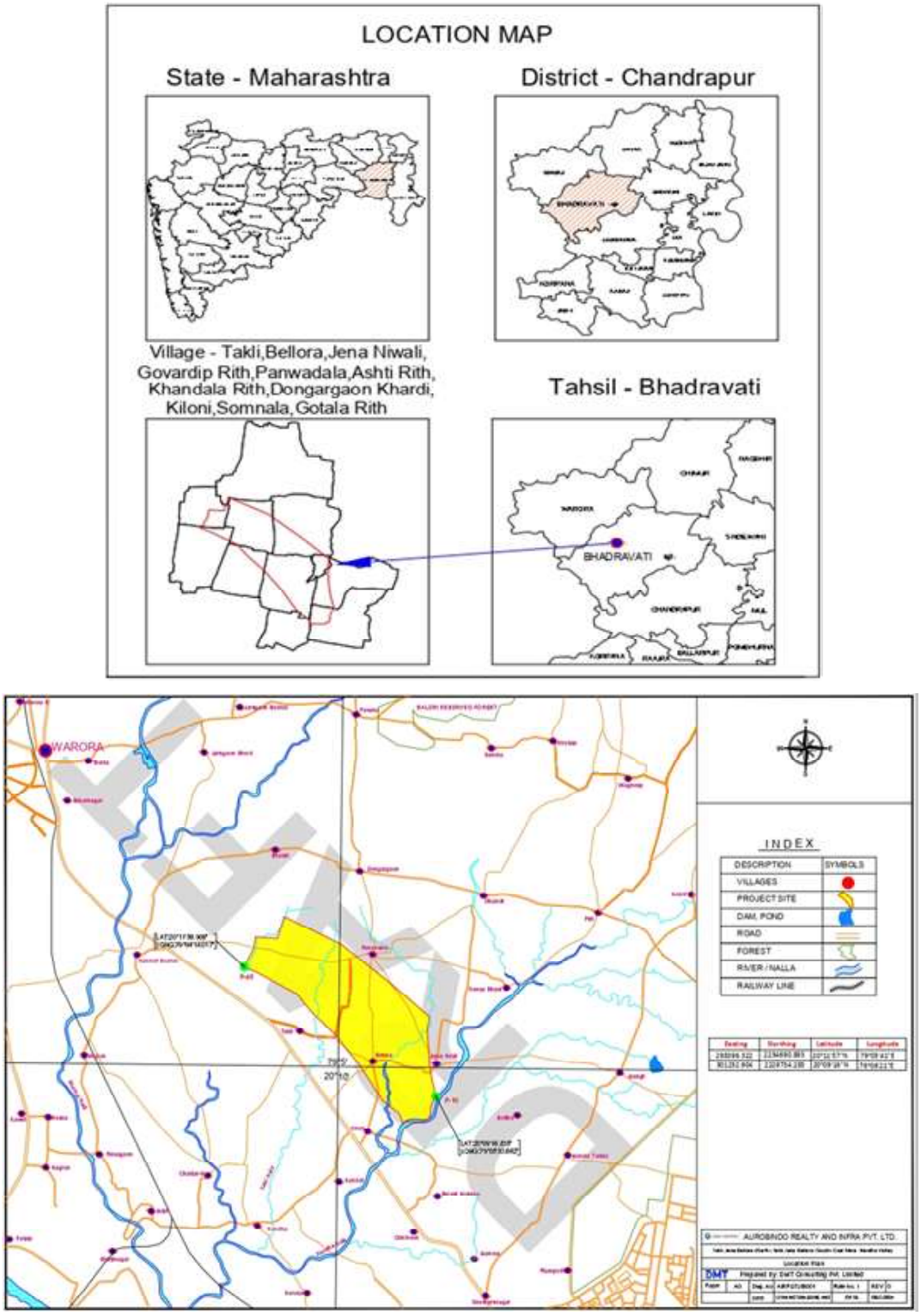

Figure 1: Location plan of the Takli Jena Bellora N-S Coal Mine Project

EXPERIMENTAL BLAST DETAILS

A total of 14 trial blasts were conducted during the field visit. All these blasts were conducted on the top, middle, and bottom benches facing east of the mine. The blast hole diameter in all the blasts was 160 mm. The number of holes fired in each round varied from 6 to 134. The burden and spacing in all the blasts ranged from 3.0 to 5.0 m and 3.0 to 6.0 m, respectively. Hole depth varied between 2.5 and 6.0 m. The average charge per hole in all the blast holes was kept between 6.25 kg and 25.0 kg. The top stemming column of the hole was kept between 2.0 and 5.4 m. The total explosives detonated in all the blasts ranged from 37.5 to 2930 kg.

Solar-made electronic detonators were used as initiation devices due to their higher reliability and safety, attributed to their rugged and proven construction. These detonators are fully programmable, allowing any delay between 0 and 8000 milliseconds. Details of all the blasts conducted during the visit are provided in **Table 1**. The firing pattern of one of the blasts is shown in **Figure 2**.

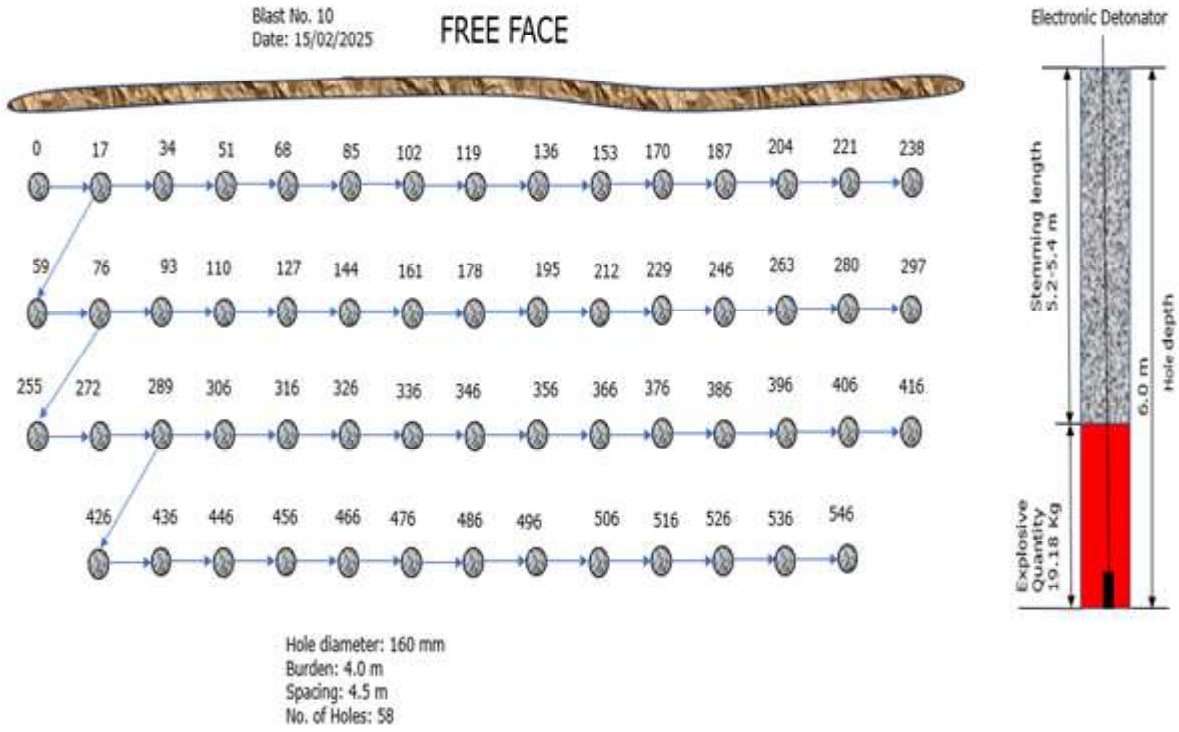

Figure 2: Charging and Firing patterns of blastholes used during experimental blasts at Takli Jena Bellora North South Coal Mine Project

MONITORING OF BLAST INDUCED GROUND VIBRATION

Ground vibration generated from the experimental blasts were recorded on the ground surface using three digital seismographs from M/s Instantel Inc., Canada. In all the blasts, the instruments were placed behind the blast face, facing Bellora village. In some of the blasts, two of the instruments were placed on Bellora village road and the residential houses to assess the impact of vibration on nearby residential structures. The locations of the vibration monitoring points are shown in **Figures 3**.

Table 1: Details of the experimental blast design parameters conducted at Takli Jena Bellora North South Coal Mine Project

S. No.	Date	Location of Blast & Strata	Hole Diameter [mm]	Average Hole Depth [m]	Total number of holes	Burden × Spacing [m]	Top stemming column [m]	Average charge per hole [Kg]	Total Explosive charge [kg]	Maximum charge per delay [kg]
1.	12-02-2025	N-E Facing Middle Bench	160	6	134	4.0 × (5.0-5.5)	4.5 – 5.0	21.87	2930	44.0
2.	12-02-2025	N-E Facing Middle Bench	160	6	50	4.0 × 4.5	4.0 – 4.5	20.72	1036	31.25
3.	13-02-2025	East Facing Middle Bench	160	6	39	(4.0 – 4.5) × (5.0 -5.3)	4.5 – 5.0	21.87	852	22
4.	13-02-2025	East Facing Middle Bench	160	6	75	(4.0 – 4.5) × (5.0 -5.3)	4.5 – 5.0	21.87	1640	22
5.	13-02-2025	East Facing Middle Bench	160	6	29	(4.5 – 5.0) × 5.0	4.5 – 5.0	25	725	25
6.	13-02-2025	East Facing Middle Bench	160	6	9	4.0 × 5.0	5.5	9.37	84	10
7.	14-02-2025	East Facing Middle Bench	160	5.5 – 6.0	53	4.0 × 4.5	4.7 – 5.3	18.75	994	19
8.	14-02-2025	East Facing Middle Bench	160	2.5 – 4.0	34	4.0 × (4.0 – 4.5)	2.0 – 3.5	9.37	319	10
9.	14-02-2025	East Facing Middle Bench	160	2.5 – 3.0	31	4.0 × (4.0 – 4.5)	2.0 – 2.5	6.25	194	6.25
10.	15-02-2025	East Facing Middle Bench	160	6	58	4.0 × 4.5	5.2 – 5.4	19.18	1113	22
11.	15-02-2025	East Facing Middle Bench	160	6	61	(4.0 – 4.5) × (4.5 – 5.5)	5.2 – 5.4	18.75	1144	19
12.	15-02-2025	East Facing Middle Bench	160	4 - 6	21	4.0 × 4.5	3.5 – 5.4	18.14	381	19
13.	15-02-2025	East Facing Top Bench	160	3	6	3.0 × 3.0	2.6	6.25	37.5	6.25
14.	15-02-2025	East Facing Top Bench	160	3	10	3.0 × (3.0 – 6.0)	2.6	6.25	62.5	6.25

Figure 3: A view of Blast vibration monitoring in the direction of Bellora village

GROUND VIBRATION RESULTS AND OBSERVATIONS

The magnitude of ground vibration data recorded during the experimental blasts varied between 0.582 and 10.19 mm/s. The distances of vibration monitoring points from the blasting sites ranged from 100 to 607 m. The recorded blast vibration and air overpressure from the trial blasts are summarized in **Table 2**.

The maximum magnitude of ground vibration recorded during the experimental blasts was 10.19 mm/s, with a peak dominant frequency of 7.5 Hz. This blast was conducted with 75 holes, and the total explosive charge was 1,640.00 kg. The maximum explosive weight per delay was 22.00 kg. Three seismographs were used to monitor this blast; two were placed behind the blast face in the direction of Bellora village, and one was placed near the residential houses of Bellora village. A ground vibration magnitude of 10.19 mm/s was recorded at a distance of 159 m from the blasting patch. The maximum ground vibration recorded near near the residential houses of Bellora village, which is the closest house to the mine, was 1.783 mm/s, with a peak dominant frequency of 7.5 Hz. The distance of the monitoring location from the blasting patch was 521 m. The vibration recorded in all the blasts was within the safe limit as per DGMS Circular 7 of 1997.

DOMINANT FREQUENCY OF GROUND VIBRATION

The Fast Fourier Transform (FFT) analyses of all the vibration data recorded were carried out to obtain the dominant frequency content of the vibration waves. The FFT analyses results showed that the dominant frequency of ground vibration waves ranged between 3.5 and 38.63 Hz. The plot of dominant frequency v/s distance of vibration measurement is shown in **Figure 4**. In most of the cases, the peak dominant frequency falls in the range of less than 8 Hz. So, blast induced ground vibration should be restricted within 5 mm/s for safety of nearby structure not belonging to owner as per DGMS circular 7, 1997 (**Table 3**). Therefore, for better safety of the different surface structures located nearby the mine, the maximum charge weight per delay have been recommended while considering ground vibration limit as 5 mm/s.

Table 3: DGMS standard (Technical Circular Number 7 of 1997)

Type of structure	Dominant excitation frequency, Hz		
	< 8 Hz	8-25 Hz	> 25 Hz
(A) Buildings/structures not belonging to the owner			
1. Domestic houses/structures (Kuchcha, brick & cement)	5	10	15
2. Industrial buildings	10	20	25
3. Objects of historical importance and sensitive structures	2	5	10
(B) Buildings with limited span of life and belonging to owner			
1. Domestic houses/structures	10	15	25
2. Industrial buildings	15	25	50

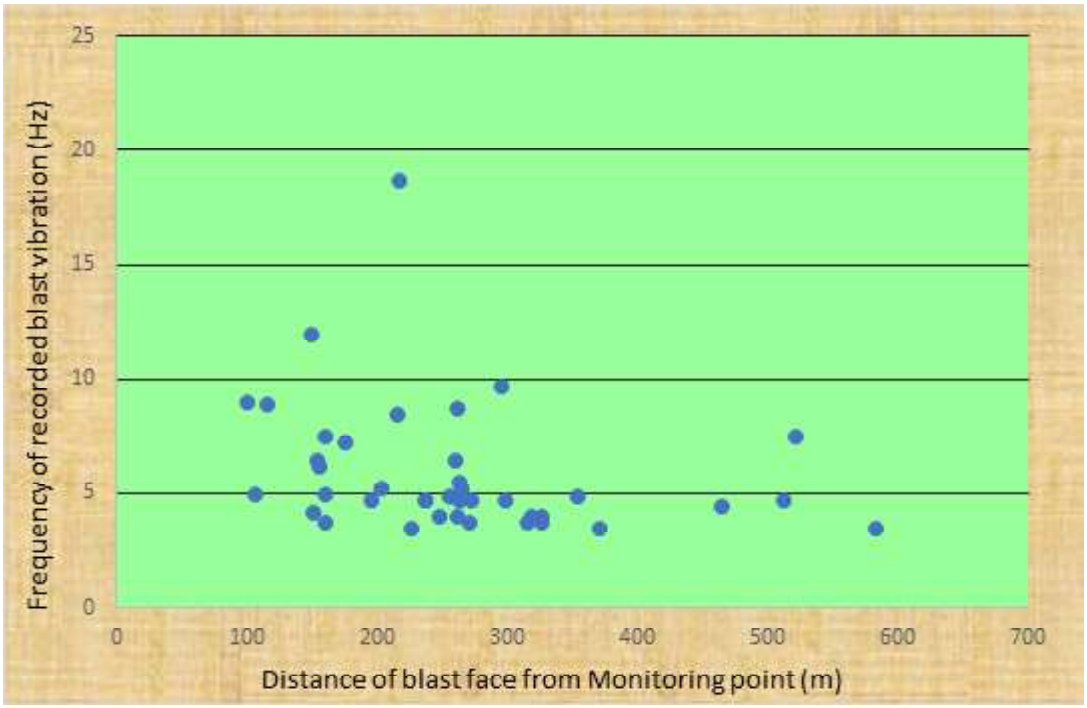

Figure 4: Plot of peak dominant frequency of blast induced ground vibration obtained from FFT analysis with their respective distance

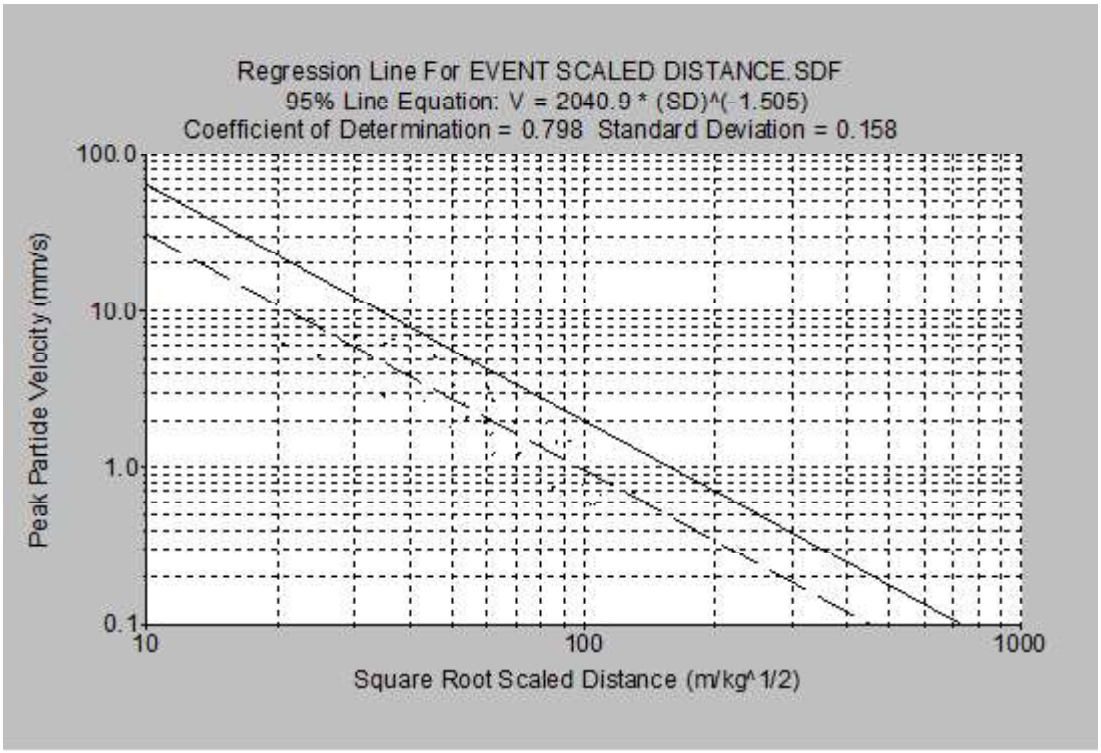

Figure 5: Regression plot of vibration data recorded at Takli Jena Bellora N-S Coal Mine Project

Table 3: Ground vibration and Air Overpressure (Noise) data recorded at Takli Jena Bellora North South Coal Mine Project

Date	Location of Blast	Max Charge per delay [kg]	Total Explosive charge [kg]	Ground Vibration and Air Overpressure (AOP)				
				Location of measurement	Distance [m]	PPV [mm/s]	Freq. (Hz)	AOP [dB(L)]
12-02-2025	N-E Facing Middle Bench	44.0	2930	Backside in the direction of Bellora Village	165	5.219	38.63	114.0
				Backside in the direction of Bellora Village	255	1.488	4.875	105.7
				Backside in the direction of Bellora Village	353	0.961	4.875	<88
12-02-2025	N-E Facing Middle Bench	31.25	1036	Backside in the direction of Bellora Village	115	6.227	8.938	127.4
				Backside in the direction of Bellora Village	195	2.898	4.688	118.4
				Backside in the direction of Bellora Village	298	2.560	4.750	<88
13-02-2025	East Facing Middle Bench	22	852	Backside in the direction of Bellora Village	214	5.141	8.5	117.4
				Backside in the direction of Bellora Village	317	3.998	4.0	<88
				North Side in Bellora Village Near Mr. Banti Matte House	582	1.374	3.5	110.2
13-02-2025	East Facing Middle Bench	22	1640	Backside in the direction of Bellora Village	159	10.19	7.5	122.4
				Backside in the direction of Bellora Village	261	4.561	8.75	<88
				North Side in Bellora Village Near Mr. Banti Matte House	521	1.783	7.5	111.2
13-02-2025	East Facing Middle Bench	25	725	Backside in the direction of Bellora Village	150	6.735	4.25	116.5
				Backside in the direction of Bellora Village	247	1.831	4.0	<88
				North Side in Bellora Village Near Mr. Banti Matte House	463	1.486	4.5	109.2
13-02-2025	East Facing Middle Bench	10	84	Backside in the direction of Bellora Village	225	1.227	3.5	104.6
				Backside in the direction of Bellora Village	314	0.778	3.75	<88
				North Side in Bellora Village Near Mr. Banti Matte House	607	NT	NT	NT
14-02-2025	East Facing Middle Bench	19	994	Backside in the direction of Bellora Village	105	8.53	5.0	117.1
				Backside near the diverted Bellora Village Road	160	6.703	5.0	110.2
				Backside in the direction of Bellora Village	263	3.226	4.75	<88
14-02-2025	East Facing Middle Bench	10	319	Backside in the direction of Bellora Village	100	3.784	9.0	112.9
				Backside near the diverted Bellora Village Road	160	3.382	3.75	108.0
				Backside in the direction of Bellora Village	260	1.933	4.0	<88
14-02-2025	East Facing Middle Bench	6.25	194	Backside in the direction of Bellora Village	175	1.923	7.25	133.3
				Backside near the diverted Bellora Village Road	216	1.462	18.75	104.2
				Backside in the direction of Bellora Village	294	0.896	9.75	<88

15-02-2025	East Facing Middle Bench	22	1113	Backside in the direction of Bellora Village	202	2.682	5.25	124.4
				Backside in the direction of Bellora Village	236	0.952	4.75	117.9
				Backside in the direction of Bellora Village	512	0.671	4.75	<88
15-02-2025	East Facing Middle Bench	19	1144	Backside in the direction of Bellora Village	236	2.083	4.75	108.8
				Backside in the direction of Bellora Village	271	1.225	4.75	112.4
				Backside in the direction of Bellora Village	370	0.742	3.50	<88
15-02-2025	East Facing Middle Bench	19	381	Backside in the direction of Bellora Village	153	6.292	6.50	118.9
				Backside in the direction of Bellora Village	262	2.906	5.50	<88
				Backside in the direction of Bellora Village	270	2.694	3.75	112.6
15-02-2025	East Facing Top Bench	6.25	37.5	Backside in the direction of Bellora Village	154	1.638	6.25	127.3
				Backside in the direction of Bellora Village	264	0.583	5.25	<88
				Backside in the direction of Bellora Village	326	1.032	4.00	119.4
15-02-2025	East Facing Top Bench	6.25	62.5	Backside in the direction of Bellora Village	149	1.967	12.00	110.5
				Backside in the direction of Bellora Village	259	0.582	6.50	<88
				Backside in the direction of Bellora Village	325	0.696	3.75	106.0

ASSESSMENT OF GROUND VIBRATION PREDICTOR EQUATION

The ground vibration data recorded at various locations during the field investigations were grouped together for statistical analysis. An empirical equation has been established correlating the maximum explosive weight per delay (Q in kg), distance of vibration measuring transducers from the blasting face (D in m) and recorded peak particle velocity (V in mm/s). The established equation for the site is:

$$V = 2040.9\, X \left(\frac{D}{\sqrt{Q}}\right)^{-1.505} \quad \text{..... (8.1)}$$

Coefficient of Determination = 0.798 & Standard Deviation = 0.158

The above equation is site specific and applicable only for the Takli Jena Bellora N-S Coal Mine Opencast Project. This equation may be used to compute the safe maximum explosive weight per delay for various distances of concerned structures. The regression plot of recorded vibration data is given in **Figure 5.**

ASSESSMENT OF SAFE VALUES OF MAXIMUM CHARGE PER DELAY

The safe level of ground vibration in terms of peak particle velocity (PPV) for the residential houses has been assessed keeping in view of the peak particle velocity of 5 mm/s as the safe level of ground vibration for the safety of nearby surface structures not belonging to owner. The safe quantities of maximum explosive weight per delay and the total explosives have been calculated for various distances from the **Equation 8.1** and are given in **Table 4.**

Table 4. Recommended explosives weight per delay to be detonated in a blasting round at Takli Jena Bellora N-S Coal Mine Project of M/s Auro Infra.

Distance of structures from the blast face [m]	Maximum explosive weight to be detonated in a delay for the safety of structures not belonging to owner considering 5 mm/s as safer limit [kg]	Maximum explosive weight to be detonated in a delay for the safety of industrial structures belonging to owner considering 10 mm/s as safer limit [kg]
100	4.0	9.0
150	8.0	20.0
200	14.0	34.0
250	22.0	54.0
300	31.0	77.0
350	42.0	105.0
400	55.0	137.0
450	69.0	173.0
500	85.0	214.0
550	103.0	258.0
600	123.0	307.0

RESULTS AND DISCUSSION

The highest recorded ground vibration magnitude was 10.19 mm/s at a monitoring distance of 159 meters. However, at a critical residential location 521 meters away, the maximum recorded vibration was 1.783 mm/s, demonstrating compliance with safety standards. The frequency analysis using Fast Fourier Transform (FFT) indicated that the dominant frequency of ground vibrations ranged between 3.5 and 38.63 Hz, with most values falling below 8 Hz. A site-specific empirical equation was developed to predict blast-induced ground vibration, allowing the calculation of safe explosive weights per delay at various distances.

CONCLUSION

The research successfully developed and validated a blast design model for safe and efficient mining operations. The controlled blasts ensured that ground vibrations levels remained within permissible limits. The established empirical equation provides a reliable tool for predicting vibration impacts and optimizing blast parameters. This research highlights the importance of precise blast design in minimizing environmental impact while maintaining operational productivity.